galaxies

MDPI

Article

The *e*MERLIN and EVN View of FR 0 Radio Galaxies

Ranieri D. Baldi [1,2,*], Gabriele Giovannini [1,3] and Alessandro Capetti [4]

[1] INAF—Istituto di Radio Astronomia, Via P. Gobetti 101, 40129 Bologna, Italy; ggiovann@ira.inaf.it
[2] School of Physics and Astronomy, University of Southampton, Southampton SO17 1BJ, UK
[3] Dipartimento di Fisica e Astronomia, Università di Bologna, Via Gobetti 93/2, 40129 Bologna, Italy
[4] INAF—Osservatorio Astrofisico di Torino, Strada Osservatorio 20, 10025 Pino Torinese, Italy; alessandro.capetti@inaf.it
* Correspondence: ranieri.baldi@inaf.it

Abstract: We present the results from high-resolution observations carried out with the *e*MERLIN UK-array and the European VLBI network (EVN) for a sample of 15 FR 0s, i.e., compact core-dominated radio sources associated with nearby early-type galaxies (ETGs), which represent the bulk of the local radio galaxy population. The 5 GHz *e*MERLIN observations available for five objects exhibit sub-mJy core components and reveal pc-scale twin jets for four out of five FR 0s once the *e*MERLIN and JVLA archival visibilities data are combined. The 1.66 GHz EVN observations available for 10 FR 0s display one- and two-sided jetted morphologies and compact cores. The pc-scale core emission contributes, on average, to about one tenth of the total extended radio emission, although we noted an increasing core contribution for flat-/inverted-spectrum sources. We found an unprecedented linear correlation between the pc-scale core luminosity ($\sim 10^{21.3}$–$10^{23.6}$ W Hz^{-1}) and [O III] line luminosity, generally considered as proxy of the accretion power, for a large sample of LINER-type radio-loud low-luminosity active nuclei, all hosted in massive ETGs, which include FR 0s and FR Is. This result represents further evidence of a common jet–disc coupling in FR 0s and FR Is, despite then differing in kpc-scale radio structure. For our objects and for other FR 0 samples reported in the literature, we estimated the jet brightness sidedness ratios, which typically range between one and three. This parameter roughly gauges the jet bulk Lorentz factor Γ, which turns out to range from 1 to 2.5 for most of the sample. This corroborates the scenario that FR 0s are characterized by mildly relativistic jets, possibly as a result of lower-spinning black holes (BHs) than the highly spinning BHs of relativistic-jetted radio galaxies, FR Is.

Keywords: radio continuum: galaxies; galaxies: active

Citation: Baldi, R.D.; Giovannini, G.; Capetti, A. The*e*MERLIN and EVN View of FR 0 Radio Galaxies. *Galaxies* **2021**, *9*, 106. https://doi.org/10.3390/galaxies9040106

Academic Editor: Wenwu Tian

Received: 29 October 2021
Accepted: 16 November 2021
Published: 18 November 2021

1. Introduction

The presence of accreting supermassive black holes (BHs) (active galactic nuclei, AGNs) at the center of local massive early-type galaxies, ETGs) has been largely reported by large-area surveys (e.g., [1–6]) and supported by theoretical studies (e.g., [7–9]). The most massive ETGs appear to be typically associated with radio-loud AGNs (RL AGNs or radio galaxies [RGs], in general) able to launch the most powerful jets in the Universe. In opposition to the latter, which have typically activity periods of 10^7–10^8 year, low-power ($\lesssim 10^{23}$ W Hz^{-1}) RGs appear to be steadily active although at a low regime [10]. From the most powerful to the weakest, RGs encompass a large range of jet properties, such as luminosities, morphologies, duty cycles, and speeds, but all sharing a single type of evolved host [11,12]. This capability of massive ETGs to be frequently associated with radio AGNs has been recently the object of several observational and theoretical studies and contextualized in the framework of AGN feedback, since RGs, even at low powers, can continuously inject energy in the central kpc of galaxies (e.g., [8,13–16]).

The vast majority of local massive ETGs are characterized by low-luminosity compact flat-spectrum radio sources (e.g., [14,17–24]). Apart from Seyferts and star-forming galaxies,

where several radio-emitting thermal and nonthermal mechanisms can co-exist [25], the majority of the most prominent flat-spectrum nuclear radio sources in nearby galaxies are found in galaxies with low-ionization nuclear emission line region (LINER) [26] nuclear spectra [27]. They are: (1) about two-thirds of the all local active galaxies [28,29]; (2) characterized by low-ionization optical forbidden lines [30] whose source of ionization has been debated for decades (low-luminosity version of bright AGNs [31], shocks [32], or stellar photoionization [33,34]); (3) powered by low-accreting radiatively inefficient discs (RIAF) [35] in the case of hosting an active BH [36]. The accretion-powered LINERs tend to host compact radio-louder cores [37–40], as the BH mass (or galaxy mass) increases (e.g., [13,41–43]). In fact, as LINERs (or in the RL regime, low-excitation radio galaxies (In the optical taxonomy of RL AGNs, RL LINERs are typically named as low-excitation radio galaxies (LERGs), while Seyferts as high-excitation radio galaxies [44,45]. LINERs and LERGs are, thus, equivalent optical classifications. Local FR Is are almost totally classified as LINERs, whereas FR IIs are associated with either LINER or Seyfert-like nuclear spectra. For example, In the Third Cambridge (3C) catalog of RGs [46], FR Is are mostly all LERGs, with only a few possible candidates of FR I HERGs, e.g., 3C 120.)) are usually radio-louder than the other optical classes and similar to low-power RGs [47–49], a model of the synchrotron self-absorbed base of a low-power jet coupled with an underluminous RIAF disc (typically in the form of an advection-dominated accretion flow (ADAF) [50–52]), analogous to the FR I disc–jet interpretation (e.g., [53,54]), has been used to describe their accretion–ejection mode. Low-luminosity LINERs have been generally interpreted as the scaled-down version of the cores of powerful RL AGNs, showing a very high brightness temperature and a flat to inverted radio spectrum that extends up to sub-mm wavelengths [55,56].

Recently, compact radio sources associated with massive ETGs with LINER nuclear spectra have been named FR 0 radio galaxies [57,58], in contrast with the other Fanaroff–Riley classes [59] because of the lack of substantial extended emissions [60–63]. FR 0s are also characterized by a core dominance, which is about 30-times higher than that of FR Is [64,65], and a poorer Mpc-scale environment (living in groups containing less than ∼15 galaxies) [66] than FR Is. FR 0s represent the most abundant population of RGs, being at least five-times more numerous than FR Is in the local Universe (redshift $z < 0.05$) [67]. Most of FR 0s have been studied at arcsec resolution with NVSS and FIRST datasets with a compact unresolved morphology. Concerning their radio-band spectral properties, their SEDs are generally flat (or flattening at higher frequencies) from hundreds of MHz (arcsec resolution with TGSS and LOFAR [68,69]) to a few GHz (sub-arcsec resolution with JVLA) and, recently, even to higher radio frequencies (∼15–22 GHz at arcmin angular resolution with a compact array or single dish [70,71]). A multifrequency JVLA followup observations of 25 FR 0s at sub-arcsec resolution revealed the presence of kpc-scale jets for about one-fourth of the sample [64,72], the first evidence of the presence of clear extended jets in FR 0s. In terms of nuclear and host properties, FR 0s are indistinguishable from FR Is (e.g., BH mass, core and bolometric luminosities, host type and mass), and in addition, FR 0s lie on the same correlation between JVLA core power and accretion power (estimated from the [O III] line and X-ray emission [64,72,73]), defined by FR Is: this clearly indicates a common central engine, where the jet is the main contributor to the whole bolometric power. At the extreme high energies, a few FR 0s (and candidates) have been detected in the γ-ray band by the Fermi Telescope [74–77] and have been proposed as possible sources of cosmic neutrinos and high-energy cosmic rays [78–80]. All these results foster the idea that the putative jets of FR 0s are possibly characterized by a relativistic bulk speed and that FR 0s may play a crucial role in galaxy evolution via a continuous low-regime jet feedback [81], as supported by numerical simulations of low-power jets (e.g., [82–84]).

Different scenarios have been suggested to account for the multiband properties of FR 0s in relation to the other RG classes. FR 0s could be powered by a slowly spinning BHs [64,85], limiting the amount of extracted energy available to launch and power the jet, thus resulting in compact, weak jets. FR 0s could be early-phase FR Is and will eventually evolve into the

latter over a period of $\sim 10^8$–10^9 year [67]. FR 0 jets could be highly intermittent, switching on/off frequently during the course of their evolution [64,67,86], resulting in the absence of prominent extended jets.

One of the best ways to probe the very inner parts of the ejection mechanism in this mostly unexplored class of RGs is to study the pc-scale radio emissions with very-long baseline imaging observations (VLBI technique), with the intention of finding the smoking-gun feature of their inability to launch a fully fledged jet structure. At the parsec scale, higher-resolution radio observations of a sample of FR 0s with world-wide VLBI, the American Very Long Baseline Array (VLBA), and the European VLBI Network (EVN) showed resolved jets of a few pc for ∼80% of the sample [87,88]. The VLBI multi-epoch data and the symmetry of the radio structures indicate that the jet bulk speeds are mildly relativistic (between 0.08c and 0.51c) with low-bulk Lorentz factors (1.7–6) and large viewing angles. However, all previous VLBI-based studies focused on particularly bright FR 0s (flux densities higher than 50 mJy, a factor 10-times higher than the typical FR 0 flux selection threshold [67]). Therefore, a comprehensive study of pc-scale radio emission in a significant and representative sample of FR 0s, moving to lower radio luminosities, is missing. Such a study would help to build an impartial view of the mechanisms of jet production in RGs, linking FR Is to FR 0s.

Together with VLBA and EVN, *e*MERLIN also provides a range of baseline lengths that permit unique studies of faint radio sources to be made over a wide range of spatial scales. In this work, we analyzed the pc-scale radio emissions of a sample of 15 low-power FR 0s with *e*MERLIN and EVN arrays.

This paper is organized as follows. In Sections 2 and 3, we present the samples, observations, and maps of the five FR 0s observed with *e*MERLIN and ten with EVN, respectively (Table 1). The main properties of the pc-scale emissions of FR 0s are presented in Section 4 and discussed in Section 5 in the context of disc–jet coupling in FR 0s in relation to other classes of RGs. We summarize the results and draw our conclusions in Section 6. Appendix A provides the *e*MERLIN and EVN map parameters.

Table 1. Column description: (1) name; (2) redshift; (3) phase calibrator of the *e*MERLIN and EVN observations; (4) BH mass ($M_\odot$); (5) [O III] line luminosity (erg s^{-1}); (6)–(9) JVLA core luminosity (erg s^{-1}), morphology (SR, slightly resolved or extended), size (kpc), and radio spectral type (S, steep; F, flat; I, inverted) with the 1.4–4.5 GHz JVLA spectral slope ($S_\nu \propto \nu^\alpha$).

Name	z	Phase Calib	M_{BH}	$L_{[O\ III]}$	L_{JVLA}	Morph	Size	Spectra ($\alpha_{1.4-4.5\ GHz}$)
				*e*MERLIN				
J2336+0004	0.076	J2335-0131	8.7	40.28	39.31	SR	1.3	S(−1.0)
J2346+0059	0.093	J2357-0152	8.3	39.96	<40.16	SR	0.5	S(−0.56)
J2357-0010	0.076	J2354-0019	8.8	40.26	39.29	SR	<0.3	S(−0.67)
J0020-0028	0.072	J0016-0015	7.6	39.97	38.93	disc	2.8	S(−0.89)
J0101-0024	0.097	J0059+0006	8.4	40.39	39.64	elongated	1.5	S(−0.45)
				EVN				
J0907+3257	0.049	J0911+3349	7.7	39.33	<39.40	disc	14	S(−1.0)
J0930+3413	0.042	J0930+3503	8.4	39.93	<39.59	SR		S(−0.49)
J0943+3614	0.022	J0945+3534	7.9	39.85	<40.3	SR		I(0.60)
J1025+1022	0.046	J1025+1253	8.9	39.48	40.62	SR		F(0.12)
J1040+0910	0.019	J1042+1203	8.3	39.54	<39.19	SR		S(−0.60)
J1213+5044	0.031	J1219+4829	8.7	40.12	40.09	two jets	2	F(−0.33)
J1230+4700	0.039	J1234+4753	8.4	40.00	40.13	SR		F(−0.29)
J1530+2705	0.033	J1539+2744	8.2	39.71	39.93	SR		F(0.19)
J1628+2529	0.040	J1628+2247	8.5	39.65	39.87	SR		F(0.11)
J1703+2410	0.031	J1659+2629	8.8	39.66	<38.85	two lobes	9	S(−0.63)

2. *e*MERLIN

2.1. Samples, Observations, and Maps

A sample of several thousands RGs selected by cross-correlating the optical SDSS and 1.4 GHz NVSS and FIRST datasets (SDSS/NVSS sample) has been recently created [89], which mostly (∼80% of the sample) consists of compact unresolved objects at the 5″-scale with FIRST [61]. This sample includes compact RGs with FIRST flux densities >5 mJy up to z ∼0.3, covering the range of radio luminosity ∼ 10^{22}–10^{26} W Hz^{-1}. Based on a JVLA followup of 12 sources in the L and C bands, [64] classified seven FR 0s based on their optical and radio properties at 1.4 GHz, 4.5 GHz, and 7.5 GHz. We proposed an *e*MERLIN observation of this sample, but only five FR 0s (named the *e*MERLIN FR 0 sample) have been observed in the C band (CY4213 project); see Table 1 (upper part).

The five sources were randomly selected from the seven FR 0s studied with JVLA [64]. Two sources appear extended a few kpc at sub-arcsec resolution with JVLA: J0020-0028 shows a twin 1″ structure, probably associated with the dusty disk of an edge-on lenticular galaxy, and J0101-0024 displays an 0.8″ elongated bent structure. The five FR 0s have FIRST flux densities in the range 5–25 mJy and are characterized by a steep radio spectra at 1.4–4.5 GHz, but a spectral flattening emerges at higher frequencies (towards 7.5 GHz). They are all hosted in red massive ETGs with BH masses $>10^{7.5}$ $M_{\odot}$.

The *e*MERLIN observations of the five FR 0s were carried our in December 2016 with six telescopes (without the Lovell telescope) spread across the U.K. (having a maximum baseline length of 217 km), reaching a nominal resolution of ∼40 mas at the C band. The observations were centered at 5 GHz with a bandwidth of 512 MHz (four spectral windows) and correlated at Jodrell Bank Observatory. The observations were divided into two observing blocks, where two or three targets were stored together with their phase and flux calibrators. We scaled the flux density using ∼15 min scans of 3C 286 and ∼10 min scans of the bandpass calibrator OQ 208 at the beginning of each run. Then, we tracked the complex antenna gains using regular ∼2.5 min scans of the bright phase reference source (see the list in Table 1), which we interleaved between 6.5 min scans on the target field, with a total target time-on-source of ∼2 h.

We calibrated the dataset with the *e*MERLIN CASA data reduction pipeline [90], which is intended to automate the procedures required in processing and calibrating radio astronomy data from the *e*MERLIN correlator. After removing the low-level RFIs with the AOFlagger software [91], we also performed a standard calibration procedure by fitting the offsets in delays using the CASA task "fringefit", by calculating the bandpass and phase solutions (see [92] for more details on the *e*MERLIN pipeline and the comparison with standard AIPS data reduction and imaging). The complex gains (phase and amplitude) were improved with several runs of self-calibration on the gain calibrators and then applied to all the targets. After a further inspection of the target data to check the quality and remove possible bad scans, the calibrated datasets were imaged (Stokes I) within the CASA environment using the task "tclean" with the deconvolver mode "mtmfs", which performs a multiscale, multifrequency synthesis algorithm [93], with a cell size of 0.013" and natural weighting. For the targets with flux densities higher than 5 mJy, we carried out a few rounds of self-calibration in phase and a final one in phase and amplitude, using 1–2 min integration times and using a 3σ minimum threshold for a valid solution.

To analyze the source parameters in the radio maps, we used the "imfit", part of the CASA "viewer", which fits two-dimensional Gaussians to an intensity distribution on a region selected interactively on the map, providing the position, deconvolved size, peak flux density, integrated flux density, and position angle (PA) of the compact source (all listed in Table A1). Whilst this procedure is valid for compact components, we estimated the total brightness of an extended component by interactively marking the region around the irregular shape of the source with CASA "viewer". Figure 1 displays the the 5 GHz maps of the five FR 0s with an angular resolution (restoring beam) of ∼40 mas and rms between 40 μJy $beam^{-1}$ and 80 μJy $beam^{-1}$.

The five sources were detected with flux densities ranging between 0.4 and 2.7 mJy beam^{-1} at 5 GHz (see Table 2). The sources appeared all slightly resolved, except J2336+0004, which showed a weak second component with PA $\sim 7°$. The angular lengths, estimated from the convolved beam major axis, considered as the largest angular scale of the source, were ∼50 mas, apart from J2336+0004, which was 0.15″: the linear physical scales correspond to ∼70–240 pc. None of the targets, even the two JVLA resolved sources (J0020-0028 and J0101-0024), showed significant evidence of jetted extended morphologies at the parsec scale.

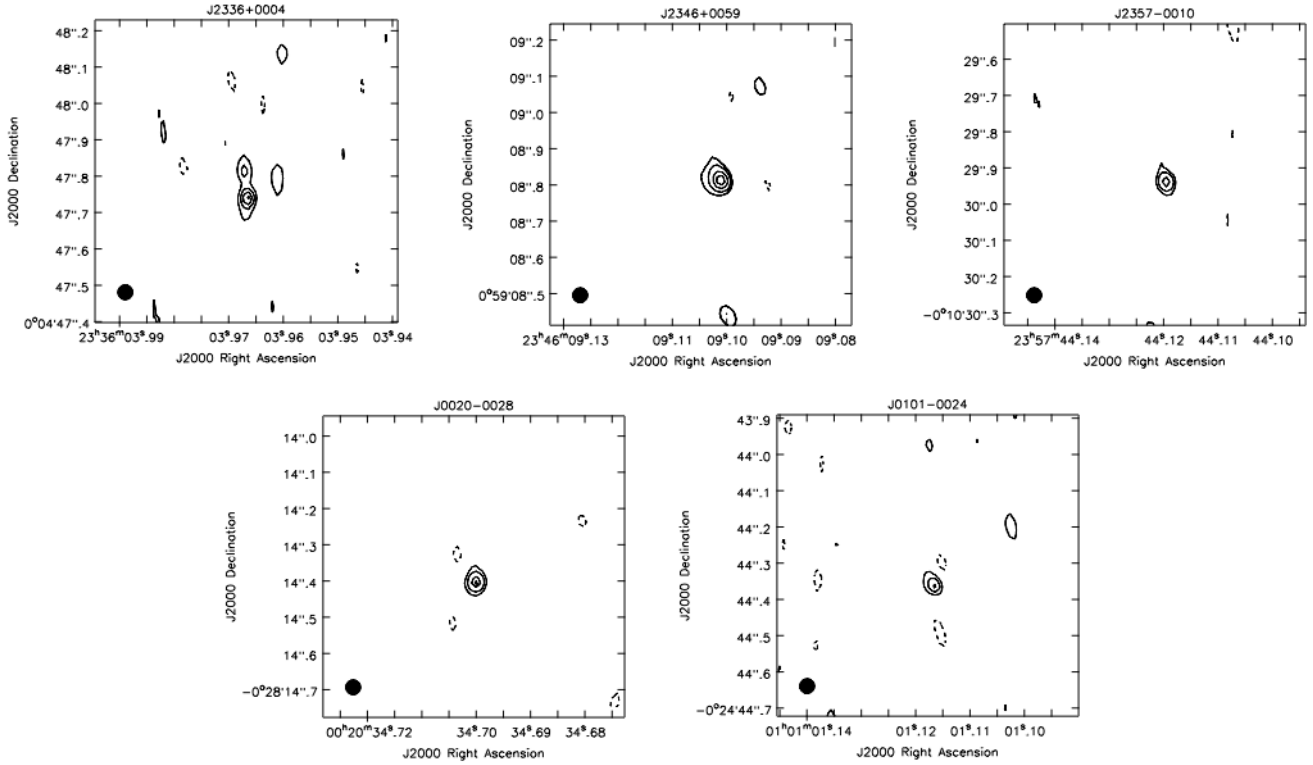

Figure 1. The 5 GHz maps of the 5 FR 0s observed with the *e*MERLIN array. The filled area, shown at the bottom-left corner of the images, represents the restoring beam of the maps. Contours and beam parameters are given in Table A1.

Table 2. Column description: (1) name; (2)–(5) core peak flux density (mJy beam^{-1}), core brightness temperature (units of 10^4 K), total core flux density (mJy), and its core luminosity (erg s^{-1}) from *e*MERLIN maps at 5 GHz; (6)–(7) radio morphology (TS, two-sided; OS, one-sided; SR, slightly resolved; UR, unresolved) and size (pc); (8) core peak flux density (mJy beam^{-1}) from the JVLA maps [64]; (9)–(10) core peak flux density (mJy beam^{-1}) and total emissions from the combined JVLA–*e*MERLIN maps; (11)–(13) PA (degree), radio morphology, and size (kpc); (14) jet sidedness.

Name	F_{core}	T_B	F_{tot}	L_{core}	M	Size	F_{JVLA}	$F_{comb\ core}$	$F_{comb\ tot}$	PA	M	Size	Jet Ratio
J2336+0004	0.64 ± 0.07	2.0	1.1	40.28	OS?	240	1.96	1.03 ± 0.04	8.5	46	TS	1.1	1.8 ± 0.2
J2346+0059	2.66 ± 0.14	8.1	3.66	39.96	SR	100	9.16	7.27 ± 0.14	13.3	29	TS	0.88	1.1 ± 0.1
J2357-0010	0.46 ± 0.16	1.4	0.47	40.26	UR	70	1.86	0.91 ± 0.03	2.0	36	TS	0.46	1.1 ± 0.1
J0020-0028	0.64 ± 0.05	2.0	0.72	39.97	UR	74	2.62	0.74 ± 0.04	1.2	−45	SR	0.30	
J0101-0024	0.38 ± 0.06	1.2	0.57	40.39	SR	120	2.5	0.82 ± 0.03	3.0	29/38	TS	1.5	1.6 ± 0.2

2.2. Combining JVLA and eMERLIN Data

Since we own the calibrated C-band JVLA observations of these five sources (carried out in 2012–2013), we combined the calibrated *e*MERLIN visibilities with those from JVLA in the same band to perform a hybrid map, obtained with long and short baselines. To match the overlapping bandwidth of two datasets, we exported the first two spectral windows of the *e*MERLIN visibilities (centered at 4816.5 MHz and 4944.5 MHz) and the

last two spectral windows of the JVLA visibilities (centered at 4819 MHz and 4947 MHz). First, we performed a first shallow reweighing of each individual visibility by its rms value with the CASA task "statwt" to contribute equally to the combined dataset given that the two radio arrays have similar image noises and antenna sizes. This process is equivalent to combining the datasets prior to Fourier transformation into the sky-plane. Both the CASA measurement sets' files were imaged simultaneously with task "tclean", using multiscale parameters [0, 5, 10] to give the best compromise between diffuse structures and unresolved sources. A further issue to solve is that the combined JVLA–*e*MERLIN beam is not a regular Gaussian due to the presence of wide shoulders owing to the short spacings provided by JVLA. Therefore, following the procedure discussed by [94], we reduced the possible flux density offsets between the combined maps and the original ones by deconvolving the combined dirty maps to deeper thresholds than those reached in the individual JVLA and *e*MERLIN maps (see the table for the typically lower rms obtained) and reweighing the data so that the resultant beam more closely represents a Gaussian. Systematic effects and complications, caused by an extreme deconvolution, can be mitigated with continuous prudent iterations [95].

Figure 2 presents the maps of the combined JVLA–*e*MERLIN datasets for the 5 FR 0s centered at 4.9 GHz with an angular resolutions less than 0.1" (see Table A1). Their rms (a few tens of μJy) are lower than that of the *e*MERLIN maps because deep self-calibration allowed reducing the noise levels and reducing the problem of the irregular combined JVLA–*e*MERLIN beam (as an exception, the combined map of J2336+0004 has a higher rms than that of the single *e*MERLIN map because the JVLA phase calibration of this target was poor [64]). All the targets appeared extended, apart from J0020-0028, where only a core with scattered components along the radio axis (PA ∼45°) was detected (the extended radio emission, consistent with the 1.4 GHz JVLA maps (PA∼40°, [64]), is visible in the dirty image, but after the deconvolution, only the core and scattered point sources remain in the final map). Two-sided jetted morphologies with extents ranging (0.2–0.8″) ∼0.3–1.5 kpc were resolved, with core components typically of 1 mJy beam^{-1}, apart from J2346+0059, which stands out for its brightness, a 7.3 mJy beam^{-1}. The twin jets detected in J2336+0004 have a PA of 46°, significantly different from what has been measured from the marginally one-sided pc-scale extent (PA ∼7°) detected with the *e*MERLIN array singularly. J0101-0024 displays two-sided structures with lobes, with a slightly convex bending of the jets (PA moving from 38° to 29° from the north to the south jets), consistent with the elongated gentle curvature noted in the JVLA map [64].

*e*MERLIN resolves the core component, probably related to the jet basis, for the five FR 0s with a core dominance F_{core}/F_{NVSS} of typically ∼6%. The apparent absence of pc-scale jets in the *e*MERLIN maps is probably due to the intrinsic weakness of their radio brightness. The kpc-scale jetted structures detected in the combined maps consist of 40–80% of the total emission and the pc-scale core components detected in full-resolution with *e*MERLIN consisting of 10–50% of the total emission detected in the combined maps.

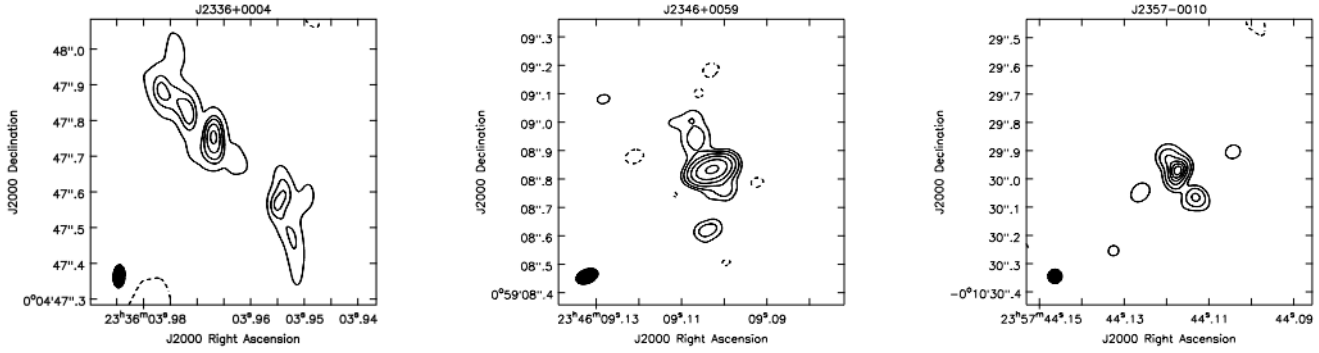

Figure 2. *Cont.*

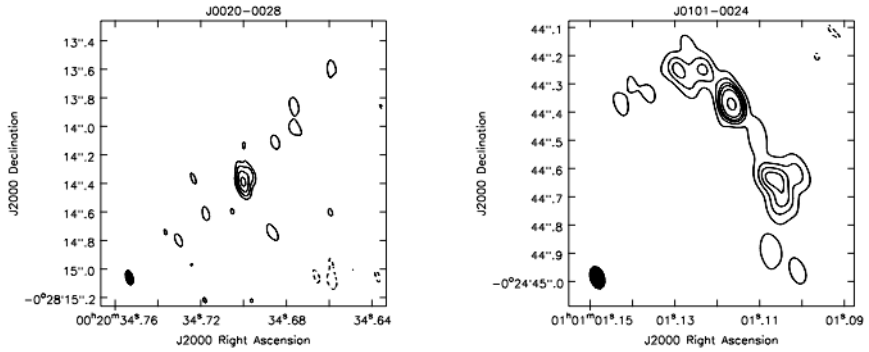

Figure 2. The 4.9 GHz maps of five FR 0s, obtained by combining the *e*MERLIN and JVLA visibilities. The filled area, shown at the bottom-left corner of the images, represents the restoring beam of the maps. Contours and beam parameters are given in Table A1.

3. EVN

Samples, Observations, and Maps

A catalog of 104 bona fide FR 0s galaxies from the SDSS/NVSS sample, named FR0CAT, was recently set [67] by including compact sources with: (1) a limit on their deconvolved angular sizes of 4″, corresponding to a linear size of ∼5 kpc, based on the FIRST images, (2) optical spectrum characteristic of LINERs, (3) red massive ETGs, and (4) $z < 0.05$. Eighteen objects were randomly extracted from the FR0CAT sample and observed with the JVLA at the L and C band in A-array configuration [72]. To study the pc-scale structure and then increase the chances of resolving the jets, ten out of these eighteen sources (see Table 1, lower panel) with JVLA flux densities at 1.4 GHz larger than 20 mJy were selected to be observed with the EVN array. These sources have BH masses ($10^{7.5}$–10^{9} $M_{\odot}$) and JVLA radio core luminosities (∼10^{39}–10^{41} erg s^{-1}) similar to those of the *e*MERLIN FR 0 subsample. Steep (but flattening at 7.5 GHz), flat, and inverted spectra in the range 1.4–4.5 GHz characterize the 10 sources [72]. Three sources reveal kpc-scale emissions in the JVLA maps: J0907+3257, similar to J0020-0028, exhibits radio emissions from an edge-on disc component; J1213+5044 and J1703+2410 reveal genuine two-sided jets of a few kpc.

The observations of these 10 objects with EVN (EVN FR 0 sample) at 18 cm (1.66 GHz) occurred in May 2019 in phase-reference mode: the target source and a nearby phase calibrator (see list in Table 1) were observed with a ∼5 min cycle. Data were correlated at the JIVE correlator (https://jive.eu/correlator-overview 28 October 2021) in Dwingeloo, and the standard EVN pipeline [96] was used for a first calibration. These data were copied in Bologna, where a final calibration and data reduction was performed using AIPS. UV data of calibrators and target sources were examined, and bad data were flagged. A standard calibration procedure was followed: gain correlation solutions were applied to the target sources from the phase and flux calibrators. A first image was obtained with the "imagr" task in AIPS, and sources with a correlated flux density of a few mJy were self-calibrated to correct the phase only. Analogous to the method explained in Section 2.1 for the *e*MERLIN FR 0 subsample, flux densities and sizes for point-like or slightly extended sources were obtained with a Gaussian fit (CASA task "imfit"), whereas for extended sources, the flux density was measured by a flux integration over a manually selected region.

Figure 3 depicts the final maps of the 10 FR 0s observed with EVN at 1.66 GHz with a typical angular resolution of 20 mas and an rms noise level of several tens of μJy (see Table A1). All the targets were detected with total flux densities of several mJy (7.5–144 mJy), where the core component appears to be the brightest element of the structure (from one-fourth to almost the entire flux density of the total emission). In J0907+3257, which exhibits a disc-related extended emission in the JVLA maps [72], at higher resolution, we resolved a triple morphology (the third southwest component, which is the faintest

within the structure, has a peak flux density of 0.45 mJy beam^{-1}, thus detected at least at 7σ over the rms) with a PA roughly perpendicular to the kpc-scale extended emission. Most of the sources (7/10) appeared resolved in elongated structures where additional components were detected in some cases: one-sided jetted (3/7) or double or triple sources (3/7 two-sided). We abstained from the morphological classification of J1040+0910 because it showed a bent triple structure (bending from -12° to 24°), where the core position is ambiguous: in the case of the core as the brightest component of its triple structure, it can be classified as a one-sided jetted source; otherwise, if the core is the central component, it resembles a two-sided structure. Here, we assumed that its putative core is the brightest south component. The physical scales of the 10 sources varied between ∼5.4 pc and 133 pc (∼30 mas to 0.15″).

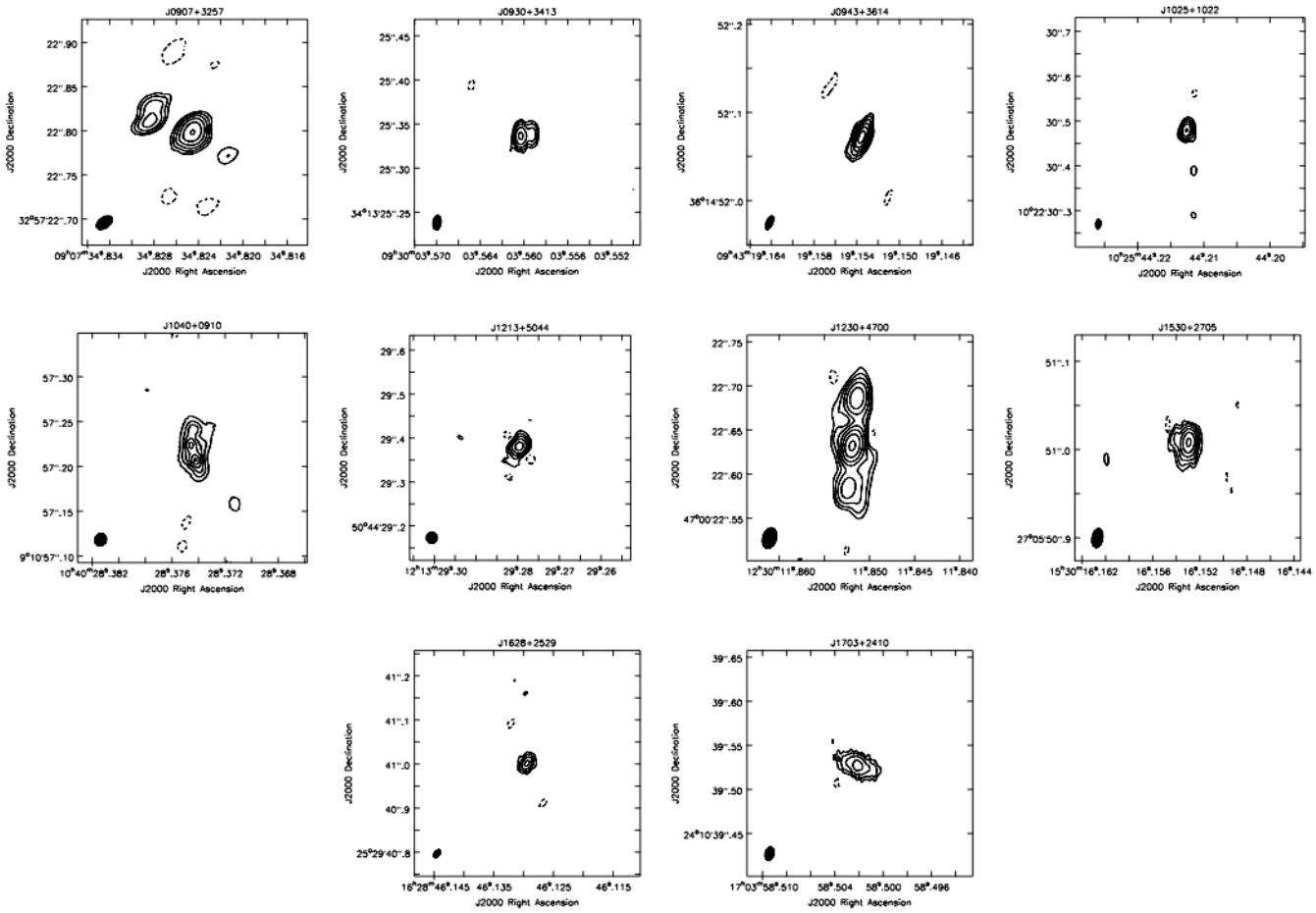

Figure 3. The 1.66 GHz EVN observations of 10 FR 0s. The filled area, shown at the bottom-left corner of the images, represents the restoring beam of the maps. Contours and beam parameters are given in Table A1.

Four of these sources have been already observed with VLBI, VLBA, and EVN at 2.3 GHz, 5 GHz, and 8.4 GHz [87,88] with an angular resolution (up to a factor of 10) higher than our observations. J0943+3614 displays a single variable unresolved component with flux densities between 130 mJy beam^{-1} and 270 mJy beam^{-1} with the VLBI [87], consistent with our EVN detection. While we detected a single core, observations with VLBA and EVN of J1025+1022 from [88] resolved a two-sided jetted shape with a core component of 60 mJy beam^{-1}, a factor ∼0.7 lower than our detection. J1213+5044 reveals a VLBA and EVN east–west twin structure of a few pc [88], included within the (51 pc-long) one-sided (PA ~ -25) morphology we detected. J1230+4700 has been observed with the VLBI, VLBA, and EVN [87,88] and shows a compact north–south two-sided morphology of a few pc, roughly aligned with the (128 pc-long) triple structure we detected.

EVN resolves the pc-scale core component of several mJy for all 10 FR 0s with a core dominance F_{core}/F_{NVSS} ranging on a large interval of values, 0.03–4, indicative of a wide variety (e.g., aligned, variable sources; see Section 5) of radio sources involved in this sample. For the resolved sources, the jet emission consists of 10–60% of the total emission, values that strongly depend on the morphology (one- or two-sided).

4. Results

Starting from their sub-arcsec JVLA compact morphologies, the 5 GHz *e*MERLIN and 1.66 GHz EVN observations of 15 FR 0s (at $z < 0.1$) have resolved their core component within an extended structure for 11 sources. The central core, which pinpoints the location of the putative BH, represents the jet base, where we can explore the mechanisms of jet launching and propagation at the parsec scale. For our FR 0 sample, the core flux densities range from sub-mJy to several tens of mJy beam^{-1}. More precisely, the EVN FR 0 sample has higher flux densities than the *e*MERLIN sample due to the selection criteria of the EVN observations. The fraction of the pc-scale core flux density with respect to the JVLA component gradually increases with the radio frequencies (note that the *e*MERLIN and EVN data are around three years later than the corresponding JVLA observations, respectively, [64] in 2012–2013 and [72] in 2016–2017), on average, from around ∼10–20% at 1.4 GHz, to 20–30% at 4.5 GHz, to 50–70% at 7.5 GHz. This suggests that a flat-spectrum core emerges from our high-resolution observation, even in the steep-spectrum sources. As an exception, the EVN core flux density of J1530+2705 is higher than those detected previously with JVLA, a hint of further processes involved (e.g., Doppler boosting, accretion/ejection variability).

The core brightness temperature of the *e*MERLIN sample is a few 10^4 K (Table 2), lower than the typical value 10^7 K, generally expected from relativistic particles emitting synchrotron emission (e.g., from jets or AGN), due to their low peak flux densities (sub-mJy beam^{-1} level). The much brighter cores and a smaller beam of the EVN sample at 1.66 GHz result in higher brightness temperatures (Table 3), i.e., 10^7–10^8 K, but lower than the nominal equipartition brightness temperature ∼10^{10} K [97] expected from a relativistic beaming of the jet.

Table 3. Column description: (1) name; (2)–(6) core peak flux density (mJy beam^{-1}), core brightness temperature (K), total core flux density (mJy), and total emission from the entire structure (mJy) and its core luminosity (erg s^{-1}) from EVN maps at 1.66 GHz; (7)–(9) PA (degree), radio morphology (TS, two-sided; OS, one-sided; SR, slightly resolved; UR, unresolved), and size (pc); (10) jet sidedness. For J1040+0910, the core location within the structure is ambiguous, and we mark with * its core flux densities and luminosity, estimated assuming its most southern brightest component as the core.

Name	F_{core}	T_B	F_{int}	F_{tot}	L_{core}	PA	Morph	Size	Jet Ratio
J0907+3257	7.61 ± 0.14	1.4×10^7	13.48 ± 0.38	19.5	39.33	60	TS	133	6.5 ± 1.0
J0930+3413	4.46 ± 0.08	1.4×10^7	5.66 ± 0.18	7.8	39.93	−86	OS	26	>2
J0943+3614	97.8 ± 0.9	3.9×10^8	128.3 ± 2.0	144	39.85		SR	5.4	
J1025+1022	84.8 ± 0.5	1.6×10^8	105.7 ± 1.0	106	39.48		UR	50	
J1040+0910	2.29 ± 0.02 *	5.6×10^6 *	4.7 ± 0.3 *	9.5	39.54 *	−12/24	?	29 pc	1.4-3
J1213+5044	50.1 ± 0.7	3.6×10^7	53.8 ± 1.3	55	40.12	−25	OS	51 pc	2.8 ± 0.2
J1230+4700	36.77 ± 0.35	4.5×10^7	37.22 ± 0.64	65.8	40.00	−7	TS	128	1.5 ± 0.1
J1530+2705	52.8 ± 1.4	9.3×10^7	57.4 ± 2.8	58.8	39.71	62	OS	22	>1
J1628+2529	21.33 ± 0.34	3.9×10^7	26.67 ± 0.71	27.0	39.65		UR	20	
J1703+2410	4.15 ± 0.06	1.2×10^7	4.72 ± 0.07	7.5	39.66	70	TS	26	1.0 ± 0.1

The most remarkable result of this study is the unprecedented concatenation of the *e*MERLIN and JVLA visibilities for five FR 0s. This procedure turned out to be a positive test to detect sub-kpc-scale jets in FR 0s when a clearly resolved jetted structure both at the arcsec- and mas-scale resolution does not emerge. Four out of five FR 0s revealed the presence of two-sided jets with radio extents ∼0.3–1.5 kpc.

Since FR 0s have been defined as compact radio sources that lack substantial extended emissions, the detection of jetted structures for most of the sources from tens of pc to kpc is surprising. The pc-scale jetted shapes are typically aligned with the JVLA jets or those detected at higher resolution by [87,88]. The radio morphologies of the pc-scale extended jets are predominantly two-sided (two-sided:one-sided = 7:3), showing lobes and plumes (J1040+0910 was excluded because of the precarious identification of the core). Among the two-sided jet group, core-brightened morphologies are more frequent (core-brightened:edge-brightened = 4:3) than the edge-brightened morphologies (triple and lobed), despite an evident difficulty in the classification due to the low brightness of the jets.

Particularly interesting are the two cases of RGs, which emit kpc-scale disc emissions probably from edge-on lenticular galaxies. At higher resolution, J0907+3257 revealed the presence of a triple structure of 133 pc with PA roughly perpendicular to the extended disc emission, whereas J0020-0028 showed scattered radio emissions along the JVLA radio structure with a northwest marginally elongated core towards the JVLA-detected twin shape.

Considering the radio spectra of the sample, we note a relation between the core dominance of the source (i.e., the ratio between the pc-scale core measured from our maps and the total radio emission measured from NVSS) and the spectral slope ($S_\nu \propto \nu^\alpha$) measured between 1.4 GHz and 4.5 GHz from the JVLA data taken from [64,72] (see Figure 4). The contribution from the core component of the total extended emission increases with the spectral flattening. This is in line with the tendency of the flat-/inverted-spectrum sources to be unresolved or one-sided jetted. In addition, it is noteworthy to point out that three sources (J0943+3614, J1025+1022, J1530+2705), which are characterized by an inverted/flat spectrum and by a substantial flux increase of their JVLA detections with respect to their NVSS-FIRST measurements by a factor of 1.6–3.2 [64,72], show a (one-sided) compact core, possibly indicating a marginal alignment of the source with the line of sight.

The pc-scale (peak) core luminosities L_{core} of the *e*MERLIN and EVN FR 0 subsamples range between $10^{21.3}$ W Hz^{-1} and $10^{23.6}$ W Hz^{-1} (integrated luminosities $\nu L_{core} \sim 10^{37.5}$–$10^{39.8}$ erg s^{-1}), a factor 10–100 weaker that the FR 0s studied by [87,88] (10^{23}–10^{24} W Hz^{-1}). The pc-scale cores detected by *e*MERLIN and EVN offer a more robust estimate of the jet base energetics than the sub-arcsec cores detected by JVLA. In this interpretation, Figure 5 represents a diagnostic plot, radio vs. [O III] luminosity, i.e., a proxy of the jet energetics vs. a proxy of the AGN bolometric luminosities (the [O III] line luminosity is a good indicator of the bolometric AGN luminosity ($L_{\rm Bol} = 3500 \times L_{[\rm O\ III]}$, [11,98]) for low-luminosity AGNs). The two quantities are expected to correlate following the radio-line relationship valid for FR 0s and FR Is [64,72], suggesting that radio emission efficiency, i.e., the fraction of the radio emission produced with respect to the AGN accretion power, is constant between FR 0s and FR Is. As we can note from Figure 5, the [O III] luminosities, $L_{[\rm O\ III]}$, of the FR 0s studied in this work, $\sim 10^{39.3}$–$10^{40.4}$ erg s^{-1}, spread in a narrower range by a factor of 10 compared to the corresponding core luminosities. This discrepancy from a one-to-one correspondence between the core and line distributions could be the result of a sharper dependence on possible Doppler flux boosting or larger core variability on parsec scales than those from a sub-arcsec view of the JVLA cores, apart from a possible flattening of the slope of the radio-line correlation. If we include the FR 0s studied with the VLBI technique by [87,88] (black stars in Figure 5), the data points cluster in limited intervals of radio and [O III] luminosities (this is because the FR 0 sample is selected at low luminosities, reaching the low-end limit of the flux-limited SDSS survey, $L_{[\rm O\ III]} \sim 10^{39}$ erg s^{-1} for galaxies at $z < 0.1$), preventing a statistical study of the presence of an L_{core}-$L_{[\rm O\ III]}$ correlation valid for FR 0s.

Since an affinity between the nuclear properties of FR 0s and FR Is has been clearly assessed [64,72,73] and low-power RGs have been found to be the scaled-down version of FR Is (e.g., [28,43,53,99,100]), it is plausible to search for a general connection between the jet and accretion strength of a population of low- and high-power RGs with comparable

properties: hosted in massive ETGs and characterized by a LINER spectrum (we excluded the FR II LINERs, because the nature of their central engine and its relation to the FR I LINERs is still not fully understood [11,101,102]). With the purpose of building such a sample of local ($z < 0.05$) LINER-type RL AGNs, we collected VLBI, VLBA, EVN, and *e*MERLIN data at 1.4 GHz and 5 GHz available from the literature ([O III] line emission from [44,103]); see Figure 5 for: LINERs from the Palomar sample of nearby galaxies [104] (green circles, from [28,105–107]), which appear as unresolved cores or core–jet structures at JVLA scales in the radio band and were classified as RL by [43]; 3C/FR Is (all LINERs, open upwards triangles, from [107–110]); and core galaxies (open downward triangles, from [28]), which have LINER spectra and are known to be miniature FR Is [100]. With the inclusion of these RL AGNs in the L_{core}-$L_{[O\ III]}$ plot, it is evident that the FR 0 data points belong to a broad sequence between the two luminosities correlated on ∼4 order of magnitudes. We fit the data points present in this sequence with a linear (in a log-log plot) relation, and we found a correlation in the form $L_{[O\ III]} \propto L_{core}^{0.72\pm0.10}$ with a Pearson correlation coefficient (r-value) of 0.782, which indicates that the two quantities do not correlate with a probability of 3×10^{-11}. This statistically robust relation corroborates the idea that nuclei of FR 0s are similar to those of LINER-like RL AGNs. The large scatter of the correlation, ∼0.27 dex, could be caused by the Doppler boosting, the nuclear variability, and the different data frequencies (particularly sensitive in the case of the steep spectrum). Furthermore, the slope of the established linear correlation is consistent with that found for nearby low-luminosity RL LINERs studied with *e*MERLIN [43]. However, a study on a large sample of FR 0s at lower radio luminosities is still needed to confirm the existence of this linear regression.

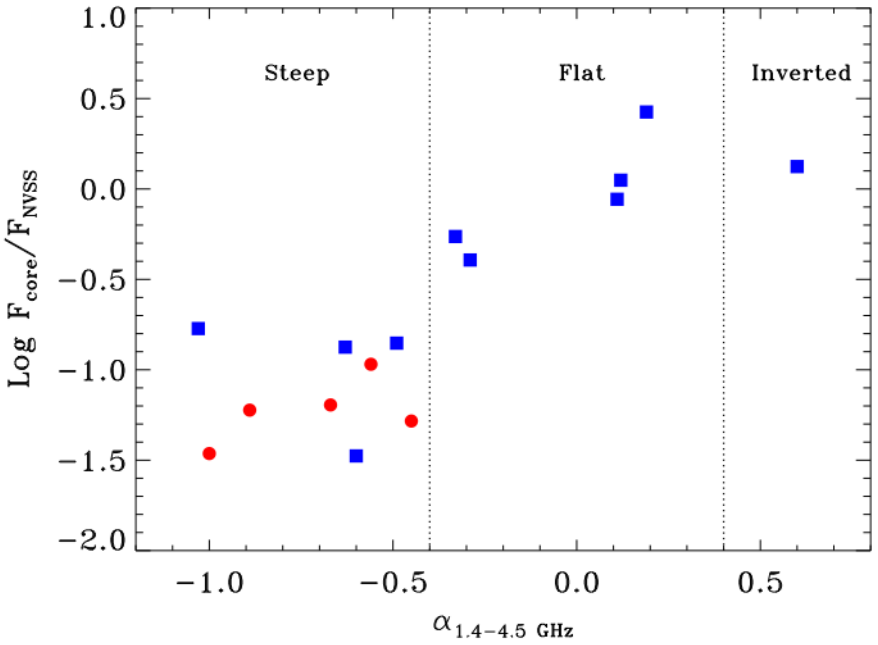

Figure 4. The 1.4–4.5 GHz spectral slope ($S_\nu \propto \nu^\alpha$) measured from the JVLA data [64,72] as a function of the core dominance, estimated as the ratio of the flux density of the pc-scale core component measured from our *e*MERLIN and EVN data and the total extended emission from NVSS flux density. Red circles mark the *e*MERLIN FR 0s and blue squares the EVN FR 0s. The vertical dashed lines denote the steep-spectrum sources ($\alpha < -0.4$), the flat-spectrum sources ($-0.4 < \alpha < 0.4$), and the inverted-spectrum sources ($\alpha > 0.4$).

With the purpose of studying the ejection mechanism in FR 0s, for the extended sources of our *e*MERLIN and EVN subsamples, we estimated the jet/counter-jet ratio by measuring the brightness ratio in two symmetric regions as near as possible to the nuclear

emission by avoiding the core and considering the surface brightness at a similar distance from the core. The jet-to-counter-jet sidedness ratios measured for the JVLA+*e*MERLIN and EVN subsamples (Tables 2 and 3) were between 1.1–1.8 and 1–3, respectively. For each source also resolved by the JVLA, the mas-scale jet ratio was higher than the corresponding value measured with JVLA at the sub-arcsec scale (in the range of 1-2 [72]). Figure 6 (upper panel) displays the pc-scale jet sidedness distribution measured from our data and from VLBI observations taken from [87,88] (we measure the jet components for the one-sided and two-sided jets at the L and C band (or the X band if the previous two bands were not available) from VLBI, VLBA, and EVN data from [87,88]). The distribution of the jet-to-counter-jet brightness ratio for our FR 0s and the sample from [87] went between 1 and 3 with one exceptional value at 6.5 (J0907+3257). The shaded histogram in Figure 6 (upper panel) represents the lower limits for the one-sided jetted sources.

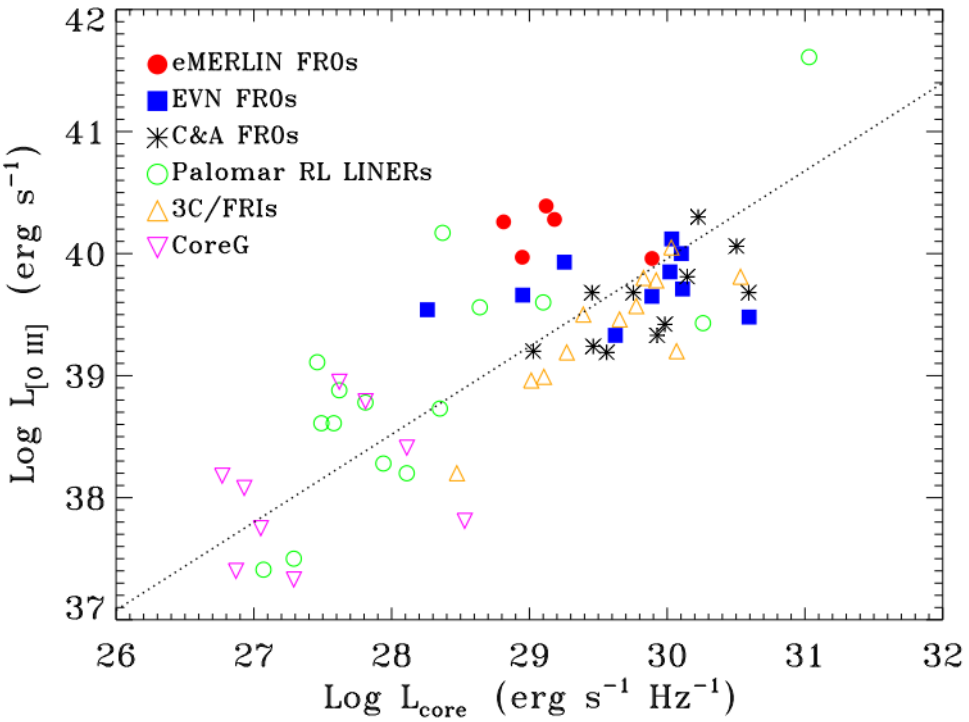

Figure 5. Parsec-scale core radio power (erg s^{-1} Hz^{-1}) vs. [O III] line luminosity (erg s^{-1}) for different samples of LINER-type RL AGNs hosted in ETGs with core-brightened morphologies (see the legend): red dots for the *e*MERLIN FR 0 subsample, blue filled squares for the EVN FR 0 subsample, black stars for FR 0s from [87,88], green empty circle for RL Palomar LINERs, upwards orange triangles for 3C/FR Is, downward pink triangles for core galaxies (see Section 4 for details). The dotted line indicates the best linear correlation found for all the sources.

From this parameter, we estimated the bulk Lorentz Γ factor of the jet following the procedure discussed by [111]. Since the jet parameters are unknown, this method assumes the value for angle θ_m that maximizes β, i.e., $\cos\theta_m = \beta$, where $\beta = v/c$ is the intrinsic jet speed, in units of c, and θ is the angle of the jet to the line of sight. With this simplification, the maximum $\Gamma_{\rm bulk}$ is:

$$\Gamma_{\rm bulk} = \left(\frac{R^m + 1}{2}\right)^{0.5} \quad (1)$$

where R is the jet sidedness and $m = k - \alpha$, where k is the parameter that accounts for the geometry of the ejecta, with $k = 2$ for a continuous jet, while α is the spectral index of the emission ($S_\nu \propto \nu^\alpha$, taken from Tables 2 and 3 and from [87,88]). With these assumptions, the range of $\Gamma_{\rm bulk}$ measured for our sample and the FR 0s from [87,88] was between ∼1 and

2.5 with two values at ∼3.5 and 12 for the targets J0933+1009 and J0907+3257, respectively (Figure 6, lower panel). We plan to re-observe these last two FR 0s with the VLBI array to check their particular extreme jet properties with respect to the rest of the sample.

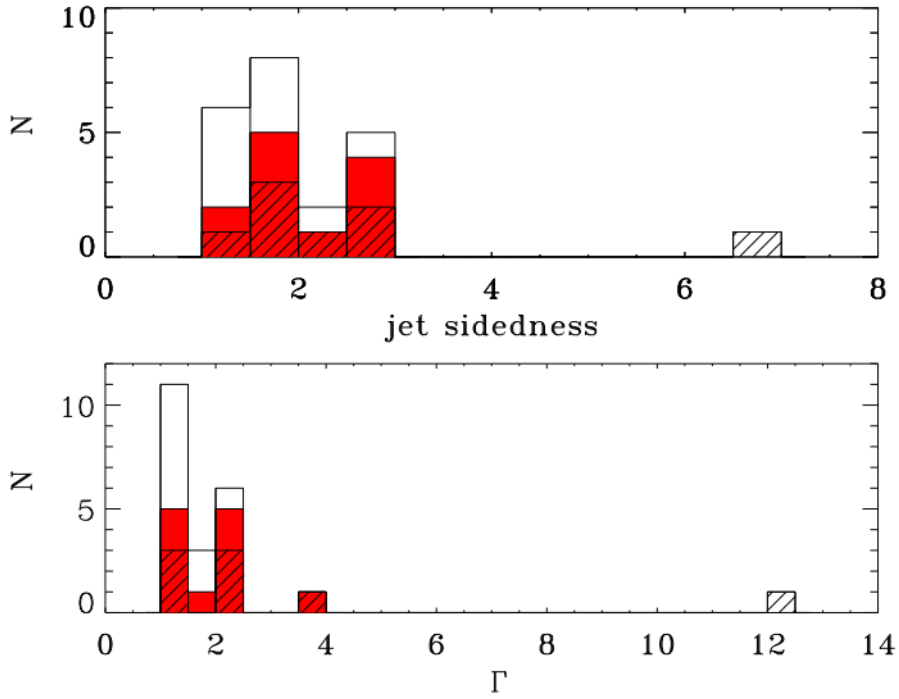

Figure 6. Upper panel: histogram of jet-to-counter-jet sidedness from our sample (white histogram) and the sample from [87,88] (red histogram) obtained from VLBI, EVN, and VLBA data. Lower panel: distribution of the jet bulk Lorentz factor Γ, estimated from the jet sidedness (see the text in Section 4). The shaded areas represent the lower limits of the jet sidedness and Γ for the one-sided sources.

5. Discussion

Our *e*MERLIN and EVN observations of 15 FR 0s confirmed the ability of this class of RGs to launch pc-scale jets, at lower luminosities ($\lesssim 10^{23}$ W Hz^{-1}) than previous VLBI studies of FR 0s. Radio structures with extents from a few tens to hundreds of pc are present for ∼86% of the FR 0s studied so far with the VLBI technique (this work and [87,88]), despite four FR 0s revealing their jetted structures only after combining the JVLA and *e*MERLIN datasets. This result eventually attests to the idea that FR 0s are genuine RGs with extended jets, although of limited size. The resolved jetted structures typically host a steep-spectrum core, while the flat-/inverted-spectrum FR 0s appear as one-sided jets or individual core components. This morphology–spectrum connection is the result of a core dominance with respect to the total emission, increasing with the flattening/inverting of the radio spectra. This highlights the power of the VLBI-based observations in resolving the pc-scale flat-spectrum core in "compact" sources such as FR 0s.

The effective capability of launching the pc scale of FR 0 jets adds up to a further similarity with classical FR Is, which generally exhibit core-brightened (however, it is correct to point out that the observed pc-scale core-brightening morphology of FR Is could be the effect of a selection bias because only FR Is with bright cores have been observed with the VLBI [107]) radio morphologies at the parsec scale [108,112,113]. At the kpc scale, about half of the FR Is show large jet asymmetries with a jet/counter-jet flux ratio larger than 2 [114,115]. At smaller scales, the jet-to-counter-jet sidedness ratio of FR Is [113,116–118] is generally larger than that measured with JVLA [119]. This morphological jet variation of FR Is at different scales is interpreted with a change of the jet bulk speed, initially from relativistic, $\Gamma > 3$, to subrelativistic speeds on kpc scales by decelerating for entrainment [120,121]. In comparison to FR Is, for the sample of 22

FR 0s studied at the parsec scale (our work and [87,88]), the jet-to-counter-jet ratio is less prominent: about one-third of FR 0s have jet sidedness larger than two. With inevitable assumptions on the jet properties, the estimated FR 0 jet bulk Γ factor, maximized to reproduce the observed distribution of jet sidedness, ranges from 1 to 2.5 for $\sim$90% of the FR 0 sample. This is in agreement with the results from [87,88] that FR 0 jets are mildly relativistic with low jet proper motions. However, a proper systematic analysis on larger samples of FR 0s matching in redshifts and luminosities with FR Is is needed to draw a final conclusion on the jet bulk speed difference between the two populations.

Another outstanding result of this study, which strengthens the connection between FR 0s and FR Is, is the presence of a broad correlation between the pc-scale core luminosities and the [O III] line luminosities, used as a proxy of the AGN strength, established for low-power LINER-like RGs, which encompass FR 0s, FR Is, and low-luminosity RL LINERs in general. This result suggests that RL LINERs, other than sharing the same type of host (massive ETGs with a BH mass $> 10^{7.5}$ $M_{\odot}$), also share a single type of central engine, able to launch (from low to high power) core-dominated jets [92,99,122] with (from mildly to highly) relativistic speeds. A radiatively inefficient accretion disc is the most plausible engine to account for the low Eddington ratios and low bolometric luminosities of FR 0s and FR Is [53,73,123]. This hypothesis is supported by the idea of an ADAF disc coupled with a jet, typically attributed to the RL LINER population in general, in agreement with previous studies (e.g., [36,43,56,124]). In fact, RIAF discs are supposed to be efficient at emanating jets, even at low energies, as suggested by theoretical studies including analytical works (e.g., [50,125,126] and numerical simulations (e.g., [127,128]).

The best scenario, which would simultaneously predict low-brightness pc-scale jets of FR 0s and a disc–jet coupling and host conditions similar to those of more powerful FR Is, but differing in large-scale environment, is a specific cosmological evolution of RGs based on BH spin and clustering. In an accretion-driven scenario, FR 0s host prograde low-spinning BHs, which will eventually evolve into highly spinning FR Is when the accreting material reaches $\sim$30% of the initial BH mass [85]. The poorer environment of FR 0s, as compared to the one of FR Is, would favor the longer stage of FR 0s due to the limited gas availability and thus would account for the larger space density of compact RGs than the extended ones [66]. Assuming a BH spin-Γ_{jet} dependence (e.g., [129,130]), the lower bulk Lorentz factor of FR 0s would be caused by their lower BH spin, limiting so their extracted energy to launch mildly relativistic jets. Instead, in a merger-driven scenario, assuming that the BH spin is the main result of a BH–BH coalescence event, in a poorer environment, major mergers of equal mass galaxies are less frequent [131,132], resulting in low probabilities of reproducing highly spinning BHs, a condition required to create extended relativistic jets. Therefore, the large-scale environment generates different merger histories and different BH spin distributions between FR 0s and FR Is, resulting eventually in a large and small population of RGs with compact and fully fledged morphologies, respectively.

While the majority of the FR 0 population conforms with the idea that they are compact core-dominated sources with mildly relativistic core-brightened jets, a small fraction exhibits different radio features from this picture. In fact, different studies at low and high radio frequencies suggested that FR 0s certainly are a mixed population of low-power radio sources, which includes genuine young RGs, such as CSSs and GPSs [58,133,134]. In our sample, we must mention that one source (J0943+3614) has an inverted spectrum, similar to what is typically seen in GHz-peaked sources [134], but previous VLBI and EVN observations of this target resolved only a core component. In addition, two sources (J0907+3257 and J1230+4700) show an mas-scale double-lobed structures consistent with the classical picture of a newly born RG. The three variable radio sources (J0943+3614, J1025+1022, J1530+2705), instead, could reconcile the picture of the aligned counterparts of FR 0s, as the BL Lacs population has been claimed as the parental population of FR 0s [135]. All these possible exceptions to the general FR 0 rule contribute to an approximately estimated $\sim$10% of contamination present in the FR 0 population [67], where young RGs, blazars,

radio-quiet AGNs, and low-luminosity compact sources (low-luminosity compact objects have been recently addressed by [136], as kpc-scale radio sources with possibly fading steep-spectrum disrupted jets and short-lived activity [137]) [58,64,133,134] would erroneously fall in the FR 0 category, if their radio–optical properties are not deeply analyzed. Nevertheless, it is possible that a genuine population of FR I progenitors or aligned weak BL Lacs whose properties have a large overlap with those of misaligned FR 0s cannot be fully disentangled from the bona fide FR 0 population.

6. Summary and Conclusions

We presented *e*MERLIN and EVN observations of a sample of fifteen FR 0s, respectively five sources at 5 GHz and ten sources at 1.66 GHz. Parsec-scale one- and two-sided jets have been detected for elven sources of the sample and cores for the remaining objects with an angular resolution of a few mas and a sensitivity of several tens of μJy.

Since we also own calibrated JVLA C-band data for the five FR 0s observed with *e*MERLIN, for the first time, we combined the visibility datasets of the two arrays in this band for this population of apparently jet-less compact RGs. This method aimed at probing the intermediate scales of the jet formation and propagation between the kpc-scale emissions lacking in FR 0s and the sub-kpc core resolved with JVLA. This procedure turned out to be successful in detecting pc-scale jets, which were missing in the two original datasets. This result means that the jets appear unresolved and resolved out, respectively, in the JVLA and *e*MERLIN maps. We can thus conclude that FR 0s, although apparently lacking extended emissions, are effectively able to emanate pc-scale jets, whose low brightness makes them hard to isolate and detect. The FR 0s, which do not show extended jets, are typically variable and/or one-sided or have an unresolved core, suggesting a possible jet orientation effect. In any case, the combination of long and short baselines represents a powerful tool to study the jet properties of the FR 0 population.

The compact component detected with mas-scale angular resolution, at the center of the resolved jetted structures of FR 0s studied with the VLBI technique, delimits the parsec-scale section of the jet along its extension. This radio-emitting region of a few pc represents a closer look at the jet-launching region and thus a better proxy of the jet energetics than previous radio studies. The core identification of FR 0s enabled us to carry out an unbiased comparison with the rest of the widely-studied population of RGs. In fact, it has been found that FR 0s, together with a homogeneous population of low-power RGs, all characterized by a LINER optical spectrum, an early-type host, and large BH masses ($>10^{7.5}$ $M_{\odot}$, satisfying the radio-loudness criteria [138]) appear to follow a broad correlation between the pc-scale core luminosities, considered as a good proxy of the jet kinetic power, and the [O III] line luminosities, indicative of the accretion power. This result sets a disc–jet connection similar to FR Is, where an RIAF disc supports the launch of a core-brightened radio structure, valid for FR 0s and generally for low-power LINER-type RGs. In conclusion, a particular set of nuclear and host properties defines a homogeneous class of RGs with a common accretion–ejection mode, from low-luminosity RL AGNs to powerful FR Is. However, although they show large differences in radio behavior from the point of view of their sizes, luminosities, and morphologies, LINER-like low-luminosity AGNs and FR 0s represent the low-end part of this continuous population distribution, which ends with fully fledged FR Is. An increasing radio luminosity, possibly due to higher BH spins or other higher values of the internal parameters (BH mass, magnetic field, etc.), would smoothly connect the low-power RGs and FR 0s to the FR Is.

Low- and high-frequency radio, optical, and X-ray observations of FR 0s have shown that FR 0s differ from FR Is in the large space density, the large-scale radio structure, and Mpc-scale environment, unlike their nuclear and host properties, which appear indistinguishable. These similarities and differences have been interpreted in the framework of RG evolution: the FR 0 state consists of a long phase of the lifetime of RGs, which inhabit moderately poor environments and are powered by low-spinning BHs, which then struggle to spin up for the low accretion rate. This scenario predicts that FR 0s are characterized

by a low jet bulk speed, assuming a linear connection between the relativistic flow of the jets and the BH spin, from which the jet energy is extracted. This interpretation is supported by our *e*MERLIN and EVN study: the bulk jet speeds of FR 0s, estimated from the pc-scale sidedness, are mostly in the range of 1–2.5, lower than typical values >3 found for FR Is. In a two-zone jet model with an inner fast spin and a slower layer [139], a weak/short (mildly) relativistic spine, which then possibly decelerates and disrupts within the galaxy via gas entrainment [120,140,141], could reconcile with the high-energy and radio properties of FR 0s [142]. Nevertheless, more dedicated studies on a statistically complete sample of FR 0s with VLBI technique observations are needed to confirm their slower jets than those of FR Is and to eventually understand the physical mechanism of jet launching/propagation in this still marginally explored class of compact RGs.

The fast approaching high-resolution and high-sensitivity radio facilities, such as the SKA [143] and the ngVLA [144], offer promising opportunities to place more stringent constraints on the jet speed and unearth a large population of FR 0s in the local Universe. The observations with these up-coming observatories will shed light on the mechanisms of accretion–ejection coupling in this abundant population of compact RGs within a general picture of an evolutionary and orientation-dependent RL AGN unification scheme.

Author Contributions: R.D.B. analyzed the *e*MERLIN data and combined the *e*MERLIN and JVLA data. G.G. analyzed the EVN dataset. R.D.B., G.G. and A.C. contributed to the discussion of the results of this work. R.D.B. wrote the article, and the co-authors gave comments and suggestions to improve the quality of the manuscript. All authors have read and agreed to the published version of the manuscript.

Funding: This research received no external funding.

Institutional Review Board Statement: Not applicable.

Informed Consent Statement: Not applicable.

Data Availability Statement: The radio data used in this work have been obtained by the *e*MERLIN and EVN arrays. Calibrated image products are available upon reasonable request to the corresponding author.

Acknowledgments: *e*MERLIN is a National Facility operated by the University of Manchester at Jodrell Bank Observatory on behalf of STFC, part of UK Research and Innovation. The European VLBI Network is a joint facility of independent European, African, Asian, and North American radio astronomy institutes. Scientific results from data presented in this publication were derived from the following EVN project code: E17C004.

Conflicts of Interest: The authors declare no conflict of interest.

Abbreviations

The following abbreviations are used in this manuscript:

RIAF	Radiatively inefficient accretion flow
RFI	Radio-frequency interference
AIPS	Astronomical Image Processing System
eMERLIN	*e*-Multi-Element Radio Linked Interferometer Network
SDSS	Sloan Digital Sky Survey
FIRST	Faint Images of the Radio Sky at Twenty centimeters survey
NVSS	National Radio Astronomy Observatory Very Large Array Sky Survey
JVLA	Jansky Very Large Array
LOFAR	Low Frequency Array
TGSS	TIFR GMRT Sky Survey
SED	Spectral energy distribution
VLBI	Very long baseline interferometry
VLBA	Very Long Baseline Array

EVN European VLBI Network
CSS Compact steep spectrum
GPS GHz-peaked source

Appendix A

We present Table A1, which provides the radio contours, the rms, and the properties of the restoring beams of the *e*MERLIN, combined JVLA–*e*MERLIN, and EVN maps of our sample.

Table A1. Column description: (1) source name; (2) FWHM of the elliptical Gaussian restoring beam (in arcsec×arcsec) of the maps from *e*MERLIN (Figure 1), combined *e*MERLIN and JVLA (Figure 2), and EVN (Figure 3); (3) PA of the restoring beam (degree); (4) contour levels (mJy beam^{-1}); (5) rms level (μJy beam^{-1}).

Name	Beam	PA	Contour Levels	rms
		*e*MERLIN		
J2336+0004	0.04 × 0.04	0.0	0.16 × (−1,1,2,3,3.9)	67
J2346+0059	0.04 × 0.04	0.0	0.36 × (−1,1,2,4,6)	80
J2357-0010	0.04 × 0.04	0.0	0.090 × (−1,1,2,4)	38
J0020-0028	0.04 × 0.04	0.0	0.12 × (−1,1,2,4,5)	40
J0101-0024	0.04 × 0.04	0.0	0.13 × (−1,1,2,3)	61
		JVLA–*e*MERLIN		
J2336+0004	0.06 × 0.03	−3.4	0.21 × (−1,1,1.5,2,3,4.5)	133
J2346+0059	0.08 × 0.05	−68.0	0.20 × (−1,1,2,4,8,16,32)	52
J2357-0010	0.05 × 0.05	0.0	0.080 × (−1,1,2,4,6,8,10)	27
J0020-0028	0.10 × 0.05	15.0	0.080 × (−1,1,2,4,8)	31
J0101-0024	0.08 × 0.05	18.0	0.059 × (−1,1,2,3,4,6,12)	21
		EVN		
J0907+3257	0.020 × 0.012	−54.0	0.23 × (−1,1,2,4,8,16,32)	61
J0930+3413	0.016 × 0.009	−8.1	0.24 × (−1,1,2,4,8,16)	33
J0943+3614	0.016 × 0.007	−23.9	2.0 × (−1,1,2,4,8,16,32)	232
J1025+1022	0.021 × 0.011	−5.4	0.98 × (−1,1,3,9,27,81)	139
J1040+0910	0.014 × 0.013	−28.0	0.39 × (−1,1,2,3,4,5,5.8)	102
J1213+5044	0.025 × 0.025	0.0	2.2 × (−1,1,2,4,8,16)	419
J1230+4700	0.024 × 0.015	−16.3	0.50 × (−1,1,2,4,8,16,32,64)	164
J1530+2705	0.021 × 0.012	−10.1	1.5 × (−1,1,2,4,8,16,32)	404
J1628+2529	0.020 × 0.012	−40.3	0.60 × (−1,1,3,9,27)	131
J1703+2410	0.015 × 0.010	−14.0	0.35 × (−1,1,2,4,8,16)	61

References

1. Boroson, B.; Kim, D.-W.; Fabbiano, G. Revisiting with Chandra the Scaling Relations of the X-ray Emission Components (Binaries, Nuclei, and Hot Gas) of Early-type Galaxies. *Astrophys. J.* **2011**, *729*, 12. [CrossRef]
2. Ferrarese, L.; Merritt, D. A Fundamental Relation between Supermassive Black Holes and Their Host Galaxies. *Astrophys. J.* **2000**, *539*, L9–L12. [CrossRef]
3. Grossová, R.; Werner, N.; Massaro, F.; Lakhchaura, K.; Plšek, T.; Gabányi, K.; Rajpurohit, K.; Canning, R.E.A.; Nulsen, P.; O'Sullivan, E.; et al. VLA Radio Study of a Sample of Nearby X-ray and Optically Bright Early-Type Galaxies. *arXiv* **2021** arXiv:2111.02430.
4. Nyland, K.; Young, L.M.; Wrobel, J.M.; Sarzi, M.; Morganti, R.; Alatalo, K.; Blitz, L.; Bournaud, F.; Bureau, M.; Cappellari, M.; et al. The ATLAS^{3D} Project—XXXI. Nuclear radio emission in nearby early-type galaxies. *Mon. Not. R. Astron. Soc.* **2016**, *458*, 2221. [CrossRef]
5. Schawinski, K.; Thomas, D.; Sarzi, M.; Maraston, C.; Kaviraj, S.; Joo, S.-J.; Yi, S.K.; Silk, J. Observational evidence for AGN feedback in early-type galaxies. *Mon. Not. R. Astron. Soc.* **2007**, *382*, 1415–1431. [CrossRef]
6. Werner, N.; McNamara, B.R.; Churazov, E.; Scannapieco, E. Hot Atmospheres, Cold Gas, AGN Feedback and the Evolution of Early Type Galaxies: A Topical Perspective. *Space Sci. Rev.* **2019**, *215*, 5. [CrossRef]

7. Croton, D.J.; Springel, V.; White, S.D.M.; De Lucia, G.; Frenk, C.S.; Gao, L.; Jenkins, A.; Kauffmann, G.; Navarro, J.F.; Yoshida, N. The many lives of active galactic nuclei: Cooling flows, black holes and the luminosities and colours of galaxies. *Mon. Not. R. Astron. Soc.* **2006** *365*, 11–28. [CrossRef]
8. Fabian, A.C. Observational Evidence of Active Galactic Nuclei Feedback. *Annu. Rev. Astron. Astrophys.* **2012**, *50*, 455–489. [CrossRef]
9. Sijacki, D.; Springel, V.; Di Matteo, T.; Hernquist, L. A unified model for AGN feedback in cosmological simulations of structure formation. *Mon. Not. R. Astron. Soc.* **2007**, *380*, 877–900. [CrossRef]
10. Sabater, J.; Best, P.N.; Hardcastle, M.J.; Shimwell, T.W.; Tasse, C.; Williams, W.L.; Brüggen, M.; Cochrane, R.K.; Croston, J.H.; de Gasperin, F.; et al. The LoTSS view of radio AGN in the local Universe. The most massive galaxies are always switched on. *Astron. Astrophys.* **2019**, *622*, A17 doi:10.1051/0004-6361/201833883. [CrossRef]
11. Heckman, T.M.; Best, P.N. The Coevolution of Galaxies and Supermassive Black Holes: Insights from Surveys of the Contemporary Universe. *Annu. Rev. Astron. Astrophys.* **2014**, *52*, 589–660. [CrossRef]
12. Morganti, R. The many routes to AGN feedback. *Front. Astron. Space Sci.* **2017**, *4*, 42. [CrossRef]
13. Best, P.N.; Kauffmann, G.; Heckman, T.M.; Brinchmann, J.; Charlot, S.; Ivezić, Ž.; White, S.D.M. The host galaxies of radio-loud active galactic nuclei: Mass dependences, gas cooling and active galactic nuclei feedback. *Mon. Not. R. Astron. Soc.* **2005**, *362*, 25–40. [CrossRef]
14. Hardcastle, M.J.; Williams, W.L.; Best, P.N.; Croston, J.H.; Duncan, K.J.; Röttgering, H.J.A.; Sabater, J.; Shimwell, T.W.; Tasse, C.; Callingham, J.R.; et al. Radio-loud AGN in the first LoTSS data release. The life-times and environmental impact of jet-driven sources. *Astron. Astrophys.* **2019**, *622*, A12. [CrossRef]
15. Hardcastle, M.J.; Croston, J.H. Radio galaxies and feedback from AGN jets. *New Astron. Rev.* **2020** *88*, 101539. [CrossRef]
16. Webster, B.; Croston, J.H.; Mingo, B.; Baldi, R.D.; Barkus, B.; Gürkan, G.; Hardcastle, M.J.; Morganti, R.; Röttgering, H.J.A.; Sabater, J.; et al. A population of galaxy-scale jets discovered using LOFAR. *Mon. Not. R. Astron. Soc.* **2021**, *500*, 4921–4936. [CrossRef]
17. Ekers, R.D.; Ekers, J.A. A survey of elliptical galaxies at 6 cm. *Astron. Astrophys.* **1973**, *24*, 247.
18. Giroletti, M.; Giovannini, G.; Taylor, G.B. Low power compact radio galaxies at high angular resolution. *Astron. Astrophys.* **2005**, *441*, 89–101.:20053347 [CrossRef]
19. Heeschen, D.S. Radio observations of E and SO galaxies. *Astron. J.* **1970**, *75*, 523. [CrossRef]
20. Kellermann, K.I.; Pauliny-Toth, I.I.K. Compact radio sources. *Annu. Rev. Astron. Astrophys.* **1981**, *19*, 373. [CrossRef]
21. Rogstad, D.H.; Ekers, R.D. Radio sources and elliptical galaxies. *Astrophys. J.* **1969**, *157*, 481. [CrossRef]
22. Sadler, E.M. Radio and optical observations of a complete sample of E and SO galaxies. III. A radio continuum survey at 2.7 and 5.0 GHz. *Astrophys. J.* **1984**, *89*, 53–63. [CrossRef]
23. Slee, O.B.; Sadler, E.M.; Reynolds, J.E.; Ekers, R.D. Parsec-scale radio cores in early-type galaxies. *Mon. Not. R. Astron. Soc.* **1994**, *269*, 928–946. [CrossRef]
24. Wrobel, J.M.; Heeschen, D.S. Radio Continuum Sources in Nearby and Bright E/S0 Galaxies: Active Nuclei Versus Star Formation. *Astrophys. J.* **1991**, *101*, 148. [CrossRef]
25. Panessa, F.; Baldi, R.D.; Laor, A.; Padovani, P.; Behar, E.; McHardy, I. The origin of radio emission from radio-quiet active galactic nuclei. *Nat. Astron.* **2019**, *3*, 387–396. [CrossRef]
26. Heckman, T.M. An optical and radio survey of the nuclei of bright galaxies. Activity in normal galactic nuclei. *Astron. Astrophys.* **1980**, *500*, 187.
27. Nagar, N.M.; Falcke, H.; Wilson, A.S.; Ho, L.C. Radio Sources in Low-Luminosity Active Galactic Nuclei. I. VLA Detections of Compact, Flat-Spectrum Cores. *Astrophys. J.* **2000**, *542*, 186. [CrossRef]
28. Nagar, N.M.; Falcke, H.; Wilson, A.S. Radio sources in low-luminosity active galactic nuclei. IV. Radio luminosity function, importance of jet power, and radio properties of the complete Palomar sample. *Astron. Astrophys.* **2005**, *435*, 521–543.:20042277. [CrossRef]
29. Saikia, P.; Körding, E.; Coppejans, D.L.; Falcke, H.; Williams, D.; Baldi, R.D.; Mchardy, I.; Beswick, R. 15 GHz radio emission from nearby low-luminosity active galactic nuclei. *Astron. Astrophys.*, **2018** *616*, A152. [CrossRef]
30. Ho, L.C. Nuclear Activity in Nearby Galaxies. *Annu. Rev. Astron. Astrophys.* **2008**, *46*, 475. [CrossRef]
31. Halpern, J.P.; Steiner, J.E. Low ionization active galactic nuclei: X-ray or shock heated? *Astrophys. J.* **1983**, *269*, L37. [CrossRef]
32. Dopita, M.A.; Sutherland, R.S. Spectral Signatures of Fast Shocks. II. Optical Diagnostic Diagrams. *Astrophys. J.* **1995**, *455*, 468. [CrossRef]
33. Binette, L.; Magris, C.G.; Stasińska, G.; Bruzual, A.G. Photoionization in elliptical galaxies by old stars. *Astron. Astrophys.* **1994**, *292*, 13.
34. Capetti, A.; Baldi, R.D. Emission lines in early-type galaxies: Active nuclei or stars? *Astron. Astrophys.* **2011**, *529*, A126. [CrossRef]
35. Narayan, R.; Yi, I. Advection-dominated Accretion: Underfed Black Holes and Neutron Stars. *Astrophys. J.* **1995**, *452*, 710. [CrossRef]
36. Falcke, H.; Körding, E.; Markoff, S. A scheme to unify low-power accreting black holes. *Astron. Astrophys.* **2004**, *414*, 895. [CrossRef]
37. Cohen, M.H.; Moffet, A.T.; Shaffer, D.; Clark, B.G.; Kellermann, K.I.; Jauncey, D.L.; Gulkis, S. Compact Radio Source in the Nucleus of M87. *Astrophys. J.* **1969**, *158*, L83. [CrossRef]

38. Falcke, H.; Nagar, N.M.; Wilson, A.S.; Ulvestad, J.S. Radio Sources in Low-Luminosity Active Galactic Nuclei. II. Very Long Baseline Interferometry Detections of Compact Radio Cores and Jets in a Sample of LINERs. *Astrophys. J.* **2000** *542*, 197–200. [CrossRef]
39. Filho, M.E.; Barthel, P.D.; Ho, L.C. The Radio Properties of Composite LINER/H II Galaxies. *Astrophys. J. Suppl. Ser.* **2002**, *142*, 223–238. [CrossRef]
40. Maoz, D. Low-luminosity active galactic nuclei: Are they UV faint and radio loud? *Mon. Not. R. Astron. Soc.* **2007**, *377*, 1696. [CrossRef]
41. Laor, A. On Black Hole Masses and Radio Loudness in Active Galactic Nuclei. *Astrophys. J.* **2000**, *543*, L111. [CrossRef]
42. Mauch, T.; Sadler, E.M. Radio sources in the 6dFGS: Local luminosity functions at 1.4 GHz for star-forming galaxies and radio-loud AGN. *Mon. Not. R. Astron. Soc.* **2007**, *375*, 931. [CrossRef]
43. Baldi, R.D.; Williams, D.R.A.; McHardy, I.M.; Beswick, R.J.; Brinks, E.; Dullo, B.T.; Knapen , J.K.; Argo, M.K.; Aalto, S.; Alberdi, A.; et al. LeMMINGs—II. The e-MERLIN legacy survey of nearby galaxies. The deepest radio view of the Palomar sample on parsec scale. *Mon. Not. R. Astron. Soc.* **2021**, *500*, 4749. [CrossRef]
44. Buttiglione, S.; Capetti, A.; Celotti, A.; Axon, D.J.; Chiaberge, M.; Macchetto, F.D.; Sparks, W.B. An optical spectroscopic survey of the 3CR sample of radio galaxies with $z < 0.3$ II. Spectroscopic classes and accretion modes in radio-loud AGN. *Astron. Astrophys.* **2010**, *509*, A6. [CrossRef]
45. Hine, R.G.; Longair, M.S. Optical spectra of 3CR radio galaxies. *Mon. Not. R. Astron. Soc.* **1979**, *188*, 111. [CrossRef]
46. Bennett, A.S. The Preparation of the Revised 3C Catalogue of Radio Sources. *Mon. Not. R. Astron. Soc.* **1962**, *125*, 75. [CrossRef]
47. Capetti, A.; Balmaverde, B. The host galaxy/AGN connection in nearby early-type galaxies. A new view of the origin of the radio-quiet/radio-loud dichotomy? *Astron. Astrophys.* **2006**, *453*, 27.:20054490. [CrossRef]
48. Kharb, P.; Capetti, A.; Axon, D.J.; Chiaberge, M.; Grandi, P.; Robinson, A.; Giovannini, G.; Balmaverde, B.; Macchetto, D.; Montez, R. Examining the Radio-loud/Radio-quiet Dichotomy with New Chandra and VLA Observations of 13 UGC Galaxies. *Astrophys. J.* **2012**, *143*, 78. [CrossRef]
49. Nagar, N.M.; Falcke, H.; Wilson, A.S.; Ho, L.C. 'Radio-loud' low luminosity AGN. *New Astron. Rev.* **2002**, *46*, 225. [CrossRef]
50. Narayan, R.; Yi, I. Advection-dominated Accretion: A Self-similar Solution. *Astrophys. J.* **1994**, *428*, L13. [CrossRef]
51. Narayan, R.; Mahadevan, R.; Quataert, E. Advection-dominated accretion around black holes. *Theory Black Hole Accretion Discs* **1998**, *148*, 182.
52. Narayan, R.; McClintock, J.E. Advection-dominated accretion and the black hole event horizon. *New Astron. Rev.* **2008** *51*, 733–751. [CrossRef]
53. Balmaverde, B.; Capetti, A.; Grandi, P. The Chandra view of the 3C/FR I sample of low luminosity radio-galaxies. *Astron. Astrophys.* **2006**, *451*, 35. [CrossRef]
54. Hardcastle, M.J.; Evans, D.A.; Croston, J.H. The active nuclei of $z < 1.0$ 3CRR radio sources. *Mon. Not. R. Astron. Soc.* **2009**, *396*, 1929.
55. Ho, L.C. The Spectral Energy Distributions of Low-Luminosity Active Galactic Nuclei. *Astrophys. J.* **1990**, *516*, 672. [CrossRef]
56. Nemmen, R.S.; Storchi-Bergmann, T.; Eracleous, M. Spectral models for low-luminosity active galactic nuclei in LINERs: The role of advection-dominated accretion and jets. *Mon. Not. R. Astron. Soc.* **2014**, *438*, 2804. [CrossRef]
57. Ghisellini, G. Extragalactic relativistic jets. *Am. Inst. Phys. Conf. Ser.* **2011**, *1381*, 180–198.
58. Sadler, E.M.; Ekers, R.D.; Mahony, E.K.; Mauch, T.; Murphy, T. The local radio-galaxy population at 20 GHz. *Mon. Not. R. Astron. Soc.* **2014**, *438*, 796. [CrossRef]
59. Fanaroff, B.L.; Riley, J.M. The morphology of extra-galactic radio sources of high and low luminosity. *Mon. Not. R. Astron. Soc.* **1974**, *167*, 31–36. [CrossRef]
60. Baldi, R.D.; Capetti, A. Radio and spectroscopic properties of miniature radio galaxies: Revealing the bulk of the radio-loud AGN population. *Astron. Astrophys.* **2009**, *508*, 603. [CrossRef]
61. Baldi, R.D.; Capetti, A. Spectro-photometric properties of the bulk of the radio-loud AGN population. *Astron. Astrophys.* **2010**, *519*, A48. [CrossRef]
62. Baldi, R.D.; Capetti, A.; Giovannini, G. The new class of FR 0 radio galaxies. *Astron. Nachr.* **2016**, *337*, 114. [CrossRef]
63. Sadler, E.M. GPS/CSS radio sources and their relation to other AGN. *Astron. Nachr.* **2016**, *337*, 105. [CrossRef]
64. Baldi, R.D.; Capetti, A.; Giovannini, G. Pilot study of the radio-emitting AGN population: The emerging new class of FR 0 radio-galaxies. *Astron. Astrophys.* **2015**, *576*, A38. [CrossRef]
65. Whittam, I.H.; Green, D.A.; Jarvis, M.J.; Riley, J.M. The faint radio source population at 15.7 GHz—IV. The dominance of core emission in faint radio galaxies. *Mon. Not. R. Astron. Soc.* **2020**, *493*, 2841. [CrossRef]
66. Capetti, A.; Massaro, F.; Baldi, R.D. Large-scale environment of FR 0 radio galaxies. *Astron. Astrophys.* **2020**, *633*, A161. [CrossRef]
67. Baldi, R.D.; Capetti, A.; Massaro, F. FR0CAT: A FIRST catalog of FR 0 radio galaxies. *Astron. Astrophys.* **2018**, *609*, A1. [CrossRef]
68. Capetti, A.; Baldi, R.D.; Brienza, M.; Morganti, R.; Giovannini, G. The low-frequency properties of FR 0 radio galaxies. *Astron. Astrophys.* **2019**, *631*, A176. [CrossRef]
69. Capetti, A.; Brienza, M.; Baldi, R.D.; Giovannini, G.; Morganti, R.; Hardcastle, M.J.; Rottgering, H.J.A.; Brunetti, G.F.; Best, P.N.; Miley, G. The LOFAR view of FR 0 radio galaxies. *Astron. Astrophys.* **2020**, *642*, A107. [CrossRef]
70. Mikhailov, A.G.; Sotnikova, Y.V. Radio Properties of FR 0 Galaxies According to Multifrequency Measurements with RATAN-600. *Astron. Rep.* **2021**, *65*, 233. [CrossRef]

71. Baldi, R.D.; Williams, D.R.A.; Capetti, A.; Giovannini, G. The AMI view of FR 0 radio galaxies. In preparation.
72. Baldi, R.D.; Capetti, A.; Giovannini, G. High-resolution VLA observations of FR0 radio galaxies: The properties and nature of compact radio sources. *Mon. Not. R. Astron. Soc.* **2019**, *482*, 2294. [CrossRef]
73. Torresi, E.; Grandi, P.; Capetti, A.; Baldi, R.D.; Giovannini, G. X-ray study of a sample of FR 0 radio galaxies: Unveiling the nature of the central engine. *Mon. Not. R. Astron. Soc.* **2018**, *476*, 5535. [CrossRef]
74. Grandi, P.; Capetti, A.; Baldi, R.D. Discovery of a Fanaroff–Riley type 0 radio galaxy emitting at γ-ray energies. *Mon. Not. R. Astron. Soc.* **2016**, *457*, 2. [CrossRef]
75. Harvey, M.; Rulten, C.B.; Chadwick, P.M. A search for γ-ray emission from a sample of local Universe low-frequency selected radio galaxies. *Mon. Not. R. Astron. Soc.* **2020**, *496*, 903. [CrossRef]
76. Paliya, V.S. A New Gamma-Ray-emitting Population of FR 0 Radio Galaxies. *Astrophys. J.* **2021**, *918*, L39. [CrossRef]
77. Stecker, F.W.; Shrader, C.R.; Malkan, M.A. The Extragalactic Gamma-Ray Background from Core Dominated Radio Galaxies. *Astropart. Phys.* **2019**, *879*, 68. [CrossRef]
78. Jacobsen, I.B.; Wu, K.; On, A.Y.L.; Saxton, C.J. High-energy neutrino fluxes from AGN populations inferred from X-ray surveys. *Mon. Not. R. Astron. Soc.* **2015**, *451*, 3649. [CrossRef]
79. Merten, L.; Boughelilba, M.; Reimer, A.; Da Vela, P.; Vorobiov, S.; Tavecchio, F.; Bonnoli, G.; Lundquist, J.R.; Righi, C. Scrutinizing FR 0 radio galaxies as ultra-high-energy cosmic ray source candidates. *Astropart. Phys.* **2021**, *128*, 102564. [CrossRef]
80. Tavecchio, F.; Righi, C.; Capetti, A.; Grandi, P.; Ghisellini, G. High-energy neutrinos from FR 0 radio galaxies? *Mon. Not. R. Astron. Soc.* **2018**, *475*, 5529. [CrossRef]
81. Ubertosi, F.; Gitti, M.; Torresi, E.; Brighenti, F.; Grandi, P. A Chandra study of Abell 795—A sloshing cluster with an FR 0 radio galaxy at its center. *Mon. Not. R. Astron. Soc.* **2021**, *503*, 4627. [CrossRef]
82. Massaglia, S.; Bodo, G.; Rossi, P.; Capetti, S.; Mignone, A. Making Faranoff-Riley I radio sources I. Numerical hydrodynamic 3D simulations of low-power jets. *Astron. Astrophys.* **2016**, *596*, A12. [CrossRef]
83. Mukherjee, D.; Bicknell, G.V.; Wagner, A.Y.; Sutherland, R.S.; Silk, J. Relativistic jet feedback—III. Feedback on gas discs. *Mon. Not. R. Astron. Soc.* **2018**, *479*, 5544. [CrossRef]
84. Mukherjee, D.; Bodo, G.; Mignone, A.; Rossi, P.; Vaidya, B. Simulating the dynamics and nonthermal emission of relativistic magnetized jets I. Dynamics. *Mon. Not. R. Astron. Soc.* **2020**, *499*, 681. [CrossRef]
85. Garofalo, D.; Singh, C.B. FR 0 Radio Galaxies and Their Place in the Radio Morphology Classification. *Astrophys. J.* **2019**, *871*, 259. [CrossRef]
86. Miraghaei, H. and Best, P.N. The nuclear properties and extended morphologies of powerful radio galaxies: The roles of host galaxy and environment. *Mon. Not. R. Astron. Soc.* **2017**, *466*, 4346. [CrossRef]
87. Cheng, X.-P.; An, T. Parsec-scale Radio Structure of 14 Fanaroff–Riley Type 0 Radio Galaxies. *Astrophys. J.* **2018**, *863*, 155. [CrossRef]
88. Cheng, X.; An, T.; Sohn, B.W.; Hong, X.; Wang, A. Parsec-scale properties of eight Fanaroff–Riley type 0 radio galaxies. *Mon. Not. R. Astron. Soc.* **2021**, *506*, 1609. [CrossRef]
89. Best, P.N.; Kauffmann, G.; Heckman, T. M.; Ivezić, Ž. A sample of radio-loud active galactic nuclei in the Sloan Digital Sky Survey. *Mon. Not. R. Astron. Soc.* **2005**, *362*, 9–24. [CrossRef]
90. Moldon, J. eMCP: E-MERLIN CASA pipeline. *Astrophys. Source Code Libr.* **2021**, *2109.006*
91. Offringa, A.R.; van de Gronde, J.J.; Roerdink, J.B.T.M. A morphological algorithm for improving radio-frequency interference detection. *Astron. Astrophys.* **2012**, *539*, A95. [CrossRef]
92. Baldi, R.D.; Williams, D.R.A.; Beswick, R.J.; McHardy, I.; Dullo, B.T.; Knapen, J.H.; Zanisi, L.; Argo, M.K.; Aalto, S.; Alberdi, A.; et al. LeMMINGs III. The e-MERLIN legacy survey of the Palomar sample: Exploring the origin of nuclear radio emission in active and inactive galaxies through the [O III]—Radio connection. *Mon. Not. R. Astron. Soc.* **2021**, *508*, 2019. [CrossRef]
93. Rau, U.; Cornwell, T.J. A multi-scale multi-frequency deconvolution algorithm for synthesis imaging in radio interferometry. *Astron. Astrophys.* **2011**, *532*, A71. [CrossRef]
94. Radcliffe, J.K.; Thomson, A.P.; Beswick R.P. Square pegs in round holes. Accurate photometry for the SKA-era. In Proceedings of the National Astronomy Meeting 2021, Bath, UK, 19–23 July 2021.
95. Radcliffe, J.K.; Beswick R.P.; Baldi, R.D.; Giovannini, G.; Capetti, A. Systematic effects and complications. In preparation.
96. Reynolds, C.; Paragi, Z.; Garrett, M. Pipeline Processing of VLBI Data. *arXiv* **2002**, arXiv:astro-ph/0205118.
97. Readhead, A.C.S. Equipartition Brightness Temperature and the Inverse Compton Catastrophe. *Astrophys. J.* **1994**, *426*, 51. [CrossRef]
98. Heckman, T.M.; Kauffmann, G.; Brinchmann, J.; Charlot, S.; Tremonti, C.; White, S.D.M. Present-day growth of black holes and bulges: The Sloan Digital Sky Survey perspective. *Astrophys. J.* **2004**, *613*, 109. [CrossRef]
99. Baldi, R.D.; Williams, D.R.A.; McHardy, I.M.; Beswick, R.J.; Argo, M.K.; Dullo, B.T.; et al. LeMMINGs—I. The eMERLIN legacy survey of nearby galaxies. 1.5 GHz parsec-scale radio structures and cores. *Mon. Not. R. Astron. Soc.* **2018**, *476*, 3478. [CrossRef]
100. Balmaverde, B.; Capetti, A. The host galaxy/AGN connection in nearby early-type galaxies. Is there a miniature radio-galaxy in every "core" galaxy? *Astron. Astrophys.* **2006**, *447*, 97. [CrossRef]
101. Macconi, D.; Torresi, E.; Grandi, P.; Boccardi, B.; Vignali, C. Radio morphology–accretion mode link in Fanaroff–Riley type II low-excitation radio galaxies. *Mon. Not. R. Astron. Soc.* **2020**, *493*, 4355. [CrossRef]
102. Tadhunter, C. Radio AGN in the local universe: Unification, triggering and evolution. *Astron. Astrophys. Rev.* **2016**, *24*, 10. [CrossRef]

103. Ho, L.C.; Filippenko, A.V.; Sargent, W.L.W. A Search for "Dwarf" Seyfert Nuclei. III. Spectroscopic Parameters and Properties of the Host Galaxies. *Astrophys. J. Suppl. Ser.* **1997**, *112*, 315. [CrossRef]
104. Ho, L.C.; Filippenko, A.V.; Sargent, W.L. A Search for "Dwarf" Seyfert Nuclei. II. an Optical Spectral Atlas of the Nuclei of Nearby Galaxies. *Astrophys. J. Suppl. Ser.* **1995**, *98*, 477. [CrossRef]
105. Anderson, J.M.; Ulvestad, J.S. The size of the radio-emitting region in low-luminosity Active Galactic Nuclei. *Astrophys. J.* **2005**, *627*, 674. [CrossRef]
106. Krips, M.; Eckart, A.; Krichbaum, T.P.; Pott, J.-U.; Leon, S.; Neri, R.; García-Burillo, S.; Combes, F.; Boone, F.; Baker, A.J.; et al. NUclei of GAlaxies. V. Radio emission in 7 NUGA sources. *Astron. Astrophys.* **2007**, *464*, 553.:20065037. [CrossRef]
107. Liuzzo, E.; Giovannini, G.; Giroletti, M.; Taylor, G.B. The Bologna complete sample of nearby radio sources II. Phase referenced observations of faint nuclear sources. *Astron. Astrophys.* **2009**, *505*, 509. [CrossRef]
108. Giovannini, G.; Taylor, G.B.; Feretti, L.; Cotton, W.D.; Lara, L.; Venturi, T. The Bologna Complete Sample of Nearby Radio Sources. *Astrophys. J.* **2005**, *618*, 635. [CrossRef]
109. Jones, D.L.; Wehrle, A.E. VLBA Imaging of NGC 4261: Symmetric Parsec-scale Jets and the Inner Accretion Region. *Astrophys. J.* **1997**, *484*, 186. [CrossRef]
110. Xu, C.; O'Dea, C.P.; Biretta, J.A. VLBI Observations of Symmetric Parsec-Scale Twin Jets in the Narrow-Angle-Tail Radio Galaxy NGC 1265 (3C 83.1B). *Astrophys. J.* **1999**, *117*, 2626. [CrossRef]
111. Bassi, T.; Migliori, G.; Grandi, P.; Vignali, C.; Pérez-Torres, M.A.; Baldi, R.D.; Torresi, E.; Siemiginowska, A.; Stanghellini, C. Faint γ-ray sources at low redshift: The radio galaxy IC 1531. *Mon. Not. R. Astron. Soc.* **2018**, *481*, 5236. [CrossRef]
112. Fanti, C.; Fanti, R.; de Ruiter, H.R.; Parma, P. VLA observations of low luminosity radio galaxies. IV. The B2 sample revisited. *Astron. Astrophys. Suppl. Ser.* **1987**, *69*, 57.
113. Venturi, T.; Castaldini, C.; Cotton, W.D.; Feretti, L.; Giovannini, G.; Lara, L.; Marcaide, J.M.; Wehrle, A.E. VLBI Observations of a Complete Sample of Radio Galaxies. VI. The Two FR I Radio Galaxies B2 0836 + 29 and 3C 465. *Astrophys. J.* **1995**, *454*, 735. [CrossRef]
114. Bridle, A.H. Sidedness, field configuration, and collimation of extra-galactic radio jets. *Astrophys. J.* **1984**, *89*, 979. [CrossRef]
115. Parma, P.; Fanti, C.; Fanti, R.; Morganti, R.; de Ruiter, H.R. VLA observations of low-luminosity radio galaxies. VI. Discussion of radio jets. *Astron. Astrophys.* **1987**, *181*, 244.
116. Giovannini, G.; Feretti, L.; Comoretto, G. VLBI Observations of a Complete Sample of Radio Galaxies. I. Snapshot Data. *Astrophys. J.* **1990**, *358*, 159. [CrossRef]
117. Giovannini, G.; Arbizzani, E.; Feretti, L.; Venturi, T.; Cotton, W.D.; Lara, L.; Taylor, G.B. Relativistic Jets in Low Power Radio Galaxies. In *International Astronomical Union Colloquium 164: Radio Emission from Galactic and Extragalactic Compact Sources*; Cambridge University Press: Cambridge, UK, 1998; Volume 144, p. 85.
118. Giovannini, G.; Cotton, W.D.; Feretti, L.; Lara, L.; Venturi, T. VLBI Observations of a Complete Sample of Radio Galaxies: 10 Years Later. *Astrophys. J.* **2001**, *552*, 508. [CrossRef]
119. Xu, C.; Baum, S.A.; O'Dea, C.P.; Wrobel, J.M.; Condon, J.J. VLBA Observations of a Sample of Nearby FR I Radio Galaxies. *Astrophys. J.* **2000**, *120*, 2950. [CrossRef]
120. Bicknell, G.V. A model for the surface brightness of a turbulent low Mach number jet. I—Theoretical development and application to 3C 31. *Astrophys. J.* **1984**, *286*, 68. [CrossRef]
121. Kharb, P.; O'Dea, C.P.; Tilak, A.; Baum, S.A.; Haynes, E.; Noel-Storr, J.; Fallon, C.; Christiansen, K. VLBA and Chandra Observations of Jets in FRI Radio Galaxies: Constraints on Jet Evolution. *Astrophys. J.* **2012**, *754*, 1. [CrossRef]
122. Capetti, A.; Massaro, F.; Baldi, R.D. FRICAT: A FIRST catalog of FR I radio galaxies. *Astron. Astrophys.* **2017**, *598*, A49. [CrossRef]
123. Balmaverde, B.; Baldi, R.D.; Capetti, A. The accretion mechanism in low-power radio galaxies. *Astron. Astrophys.* **2008**, *486*, 119. [CrossRef]
124. Chiaberge, M.; Capetti, A.; Macchetto, F.D. The Hubble Space Telescope View of LINER Nuclei: Evidence for a Dual Population? *Astrophys. J.* **2005**, *625*, 716. [CrossRef]
125. Meier, D.L. The Association of Jet Production with Geometrically Thick Accretion Flows and Black Hole Rotation. *Astrophys. J.* **2001**, *548*, L9. [CrossRef]
126. Nemmen, R.S.; Bower, R.G.; Babul, A.; Storchi-Bergmann, T. Models for jet power in elliptical galaxies: A case for rapidly spinning black holes. *Mon. Not. R. Astron. Soc.* **2007**, *377*, 1652. [CrossRef]
127. McKinney, J.C.; Tchekhovskoy, A.; Blandford, R.D. General relativistic magnetohydrodynamic simulations of magnetically choked accretion flows around black holes. *Mon. Not. R. Astron. Soc.* **2012**, *423*, 3083. [CrossRef]
128. Tchekhovskoy, A.; Narayan, R.; McKinney, J.C. Efficient generation of jets from magnetically arrested accretion on a rapidly spinning black hole. *Mon. Not. R. Astron. Soc.* **2011**, *418*, L79. [CrossRef]
129. Maraschi, L.; Colpi, M.; Ghisellini, G.; Perego, A.; Tavecchio, F. On the role of black hole spin and accretion in powering relativistic jets in AGN. *J. Phys. Conf. Ser.* **2012**, *355*, 012016. [CrossRef]
130. Tchekhovskoy, A.; Narayan, R.; McKinney, J.C. Black Hole Spin and The Radio Loud/Quiet Dichotomy of Active Galactic Nuclei. *Astrophys. J.* **2010**, *711*, 50. [CrossRef]
131. Jian, H.-Y.; Lin, L.; Chiueh, T. Environmental Dependence of the Galaxy Merger Rate in a ΛCDM Universe. *Astrophys. J.* **2012**, *754*, 26. [CrossRef]

132. Stewart, K.R.; Bullock, J.S.; Barton, E.J.; Wechsler, R.H. Galaxy Mergers and Dark Matter Halo Mergers in ΛCDM: Mass, Redshift, and Mass-Ratio Dependence. *Astrophys. J.* **2009**, *702*, 1005. [CrossRef]
133. Mikhailov, A.; Sotnikova, Y. The relationship between FR 0 radio galaxies and GPS sources 2021. *arXiv* **2021**, arXiv:2111.06141.
134. O'Dea, C.P.; Saikia, D.J. Compact steep-spectrum and peaked-spectrum radio sources. *Astron. Astrophys. Rev.* **2021**, *29*, 3. [CrossRef]
135. Massaro, F.; Capetti, A.; Paggi, A.; Baldi, R.D.; Tramacere, A.; Pillitteri, I.; Campana, R. Dragon's Lair: On the Large-scale Environment of BL Lac Objects. *Astrophys. J. Lett.* **2020**, *900*, L34. [CrossRef]
136. Kunert-Bajraszewska, M.; Thomasson, P. A survey of Low Luminosity Compact sources. *Astron. Nachr.* **2009**, *330*, 210. [CrossRef]
137. Kunert-Bajraszewska, M.; Labiano, A.; Siemiginowska, A.; Guainazzi, M. First, X-ray observations of low-power compact steep spectrum sources. *Mon. Not. R. Astron. Soc.* **2014**, *437*, 3063. [CrossRef]
138. Chiaberge, M.; Marconi, A. On the origin of radio loudness in active galactic nuclei and its relationship with the properties of the central supermassive black hole. *Mon. Not. R. Astron. Soc.* **2011**, *416*, 917. [CrossRef]
139. Ghisellini, G.; Tavecchio, F.; Chiaberge, M. Structured jets in TeV BL Lac objects and radiogalaxies. Implications for the observed properties. *Astron. Astrophys.* **2005**, *432*, 401. [CrossRef]
140. Laing, R.A. Large Scale Structure: Jets on kiloparsec Scales (Review). *Extragalact. Radio Sources* **1996**, *175*, 147.
141. Laing, R.A.; Bridle, A.H. Systematic properties of decelerating relativistic jets in low-luminosity radio galaxies. *Mon. Not. R. Astron. Soc.* **2014**, *437*, 3405. [CrossRef]
142. Baldi, R.D.; Torresi, E.; Migliori, G.; Balmaverde, B. The High Energy View of FR0 Radio Galaxies. *Galaxies* **2019**, *7*, 76. [CrossRef]
143. Kapinska, A.D.; Hardcastle, M.; Jackson, C.; An, T.; Baan, W.; Jarvis, M. Unravelling lifecycles and physics of radio-loud AGN in the SKA Era. In Proceedings of the Advancing Astrophysics with the Square Kilometre Array (AASKA14), Giardini Naxos, Italy, 9–13 June 2014; Volume 2015, p. 173
144. Nyland, K.; Harwood, J.J.; Mukherjee, D.; Jagannathan, P.; Rujopakarn, W.; Emonts, B.; Alatalo, K.; Bicknell, G.V.; Davis, T.A.; Greene, J.E.; et al. Revolutionizing Our Understanding of AGN Feedback and its Importance to Galaxy Evolution in the Era of the Next Generation Very Large Array. *Astrophys. J.* **2018**, *859*, 23. [CrossRef]